# **Mathematical Biology**



# Mixed uncertainty analysis on pumping by peristaltic hearts using Dempster–Shafer theory

Yanyan He<sup>1</sup> · Nicholas A. Battista<sup>2</sup> · Lindsay D. Waldrop<sup>3</sup>

Received: 1 February 2024 / Revised: 22 May 2024 / Accepted: 4 June 2024 © The Author(s), under exclusive licence to Springer-Verlag GmbH Germany, part of Springer Nature 2024

#### **Abstract**

In this paper, we introduce the numerical strategy for mixed uncertainty propagation based on probability and Dempster–Shafer theories, and apply it to the computational model of peristalsis in a heart-pumping system. Specifically, the stochastic uncertainty in the system is represented with random variables while epistemic uncertainty is represented using non-probabilistic uncertain variables with belief functions. The mixed uncertainty is propagated through the system, resulting in the uncertainty in the chosen quantities of interest (QoI, such as flow volume, cost of transport and work). With the introduced numerical method, the uncertainty in the statistics of QoIs will be represented using belief functions. With three representative probability distributions consistent with the belief structure, global sensitivity analysis has also been implemented to identify important uncertain factors and the results have been compared between different peristalsis models. To reduce the computational cost, physics constrained generalized polynomial chaos method is adopted to construct cheaper surrogates as approximations for the full simulation.

**Keywords** Aleatory and epistemic uncertainties · Generalized polynomial chaos · Sensitivity analysis · Dempster–Shafer theory · Peristaltic pumping model · Immersed boundary method

✓ Yanyan He yanyan.he@unt.edu

Nicholas A. Battista battistn@tcnj.edu

Lindsay D. Waldrop waldrop@chapman.edu

Published online: 16 June 2024

- Department of Mathematics, and of Computer Science and Engineering, University of North Texas, 1155 Union Circle, Denton, TX 76203, USA
- Department of Mathematics and Statistics, The College of New Jersey, Pennington Rd, Ewing Township, NJ 08618, USA
- Schmid College of Science and Technology, Chapman University, One University Drive, Orange, CA 92866, USA



13 Page 2 of 33 Y. He et al.

#### Mathematics Subject Classification #41 $\cdot$ #60 $\cdot$ #92

#### 1 Introduction

A key feature in understanding many biological functional systems is how that system behaves with respect to the variation of parameters (parametric uncertainty). Most systems in biology are complex and nonlinear, meaning that changes in a parameter, whether it is a morphological feature or kinematic quantity, could have outsized effects on the performance of that system (Wainwright et al. 2005; Anderson and Patek 2015). With the application of detailed computational modeling, such as that found with computational fluid dynamics (CFD), assessing uncertainty in models becomes highly important to understanding (1) how the system as a whole functions in real-world conditions, and (2) how the system has evolved over time (Wainwright 2007; Anderson and Patek 2015; Polly et al. 2016; Muñoz 2019).

Traditionally, uncertainty has been characterized using random variables/processes in the framework of probability theory, and various probabilistic uncertainty quantification (UQ) methods such as the Monte Carlo (MC) method, generalized polynomial chaos (gPC) expansion, and the stochastic collocation method (Wiener 1938; Xiu and Karniadakis 2002; Mathelin and Hussaini 2003; He et al. 2018; Schobi et al. 2015) have been developed. These methods have been applied to various biological systems. For example, different variations of Monte Carlo sampling techniques have been used within Bayesian methods to obtain the posterior distribution of the parameters in a computational model of molecular mechanisms of signaling (Mitra and Hlavacek 2019). Quarteroni et al. have applied Monte Carlo sampling method to quantify the uncertainty in model output propagated from uncertain parameters in the cardiovascular system (Quarteroni et al. 2017). Hu et al. have proposed to use the gPC expansion to quantify parametric uncertainty in ion channel models of mouse ventricular cell and further propagate the uncertainty across different organizational levels of cell and tissue (Hu et al. 2018). Our previous work has also applied gPC method for uncertainty quantification in peristaltic pumping by valveless, tubular heart (Waldrop et al. 2020k).

However, in practice, the system may consist of uncertain parameters, whose uncertainty is epistemic (referring to the uncertainty due to the lack of knowledge) rather than aleatory (referring to the uncertainty due to the random nature). For example, Regan et al. have provided examples from ecology and conservation biology regarding the uncertainty due to subjective judgment, that occurs as a result of interpretation of insufficient empirical data (Regan et al. 2002). In such scenario, non-probabilistic approaches based on the alternative mathematical frameworks (such as interval analysis, fuzzy set theory (Zadeh 1965; Walley and Cooman 2001), possibility theory (Dubois and Prade 1988; Dubois 2006), generalized *p*-boxes (Destercke et al. 2008), and Dempster–Shafer (DS) theory (Shafer 1976; Dempster 1967)) may provide a better representation of the epistemic uncertainty (Oberkampf et al. 2001; Jakeman et al. 2010; Chen et al. 2015; He et al. 2015; Wang et al. 2015; Baudrit et al. 2006; Roy and Oberkampf 2011; Lockwood et al. 2012). DS theory can be considered as a generalization of probability theory and various applications have adopted DS theory based



epistemic uncertainty propagation techniques in the literature (Talavera et al. 2013; Tang et al. 2015; Abdallah et al. 2013; Bae et al. 2003). The application of DS theory to biological field also has a long history. In 1980s, Atkinson and Gammerman had proposed an application of expert system technology based DS theory to the problem of biological identification (Atkinson and Gammerman 1987). In the current work, we will focus on the uses of DS theory for epistemic uncertainty quantification.

As concluded in Regan et al. (2002), uncertainties from different sources in any application will compound. In other words, mixed types of uncertainties often exist simultaneously in the underlying physical system and the simulation models. Therefore the numerical UQ techniques for mixed aleatory and epistemic uncertainty propagation also need to be explored. There are previous studies in the literature that have attempted to deal with mixed uncertainty (Roy and Oberkampf 2011; Eldred et al. 2011; Baudrit et al. 2006; Shah et al. 2015). For example, Roy and Oberkampf have estimated the predictive uncertainty of scientific computing applications using a comprehensive framework based on the combination of probability theory and interval analysis to produce a p-box to represent mixed types of uncertainties in the model output (Roy and Oberkampf 2011). Eldred et al. have discussed the mixed UQ methods based on the interval-valued probability, second-order probability and DS theory combined with probability theory where stochastic expansion methods are applied in stochastic space for the reduction of computational cost (Eldred et al. 2011). Tang et al. have combined gPC method and DS theory to quantify the mixed types of uncertainty in synthetic problems, where gPC method deals with aleatory uncertainty and DS theory is for epistemic uncertainty (Tang et al. 2010). He and Hussaini have defined a distance measure based on the well-known Hausdorff distance to determine the difference between two BBAs and provided rigorous error analysis of the mixed UQ approach based on DS theory (He and Hussaini 2023).

As the development of mixed UQ techniques, their application to various disciplines starts to draw attention. For example, Wang et al. have dealt with mixed types of uncertainty in thermal structure design with reliability-based optimization (Wang et al. 2017). He et al. have applied mixed UQ tools to quantify the uncertainty in the spatial location of an isocontour for the electric potential field over a 2D torso slice, obtained by solving an electrocardiographic forward problem (He et al. 2015). However, the research on mixed uncertainty propagation through the simulation models of biological systems, especially tubular heart pumping system, is still very limited. Therefore, one of our objectives is to quantify the mixed types of uncertainty in the computational models of peristalsis. Specifically, we will adopt a MC sampling method to deal with the aleatory uncertainty while using DS theory-based approach to deal with epistemic uncertainty. To reduce the computational cost, we have implemented gPC expansion method to construct cheaper surrogate to approximate the full simulation.

With the constructed surrogate, we further analyze the influence of uncertain input factors on the uncertainty in quantities of our interest using sensitivity analysis (SA). The SA methods can be broadly categorized into two types: local sensitivity analysis that investigates the impact on the model output based on the small perturbation of input variables only very close to a fixed points (such as the nominal values), and global sensitivity analysis that explores the impact on the model output based on the uncertainty of the input variables over the whole parameter space (Marino



13 Page 4 of 33 Y. He et al.

et al. 2008). When the parameter space is large where the uncertainty cannot be considered as the small perturbations around the nominal values, global sensitivity analysis might be more suitable to identify the "important" parameters. There are different indices proposed for different mathematical models to measure the global sensitivity in the literature. For example, standardized regression coefficients (SRC) can be used for linear functions, and partial rank correlation coefficients (PRCC) works well for nonlinear but monotonic relationships between outputs and inputs (Marino et al. 2008). For nonlinear non-monotonic functions, variance-based SA such as Sobol' indices can be the best choice (Sobol' 1993). Here, we adopt Sobol' indices to measure the global sensitivity for the complex and nonlinear biological system under our consideration. Sobol' indices have been heavily used in the framework of probability theory (Arachchilage et al. 2023; He et al. 2020; Waldrop et al. 2020k, 2018; Kiparissides et al. 2008; Randall et al. 2021; Jarrett et al. 2015), however, its application to the systems with epistemic uncertainty is very limited due to the lack of availability of probability density functions for uncertain parameters. Therefore, another objective of our current work is to analyze the sensitivity for peristalsis models involving both aleatory and epistemic uncertainties. Specifically, we will adopt the exploratory SA method (Helton et al. 2006a), which is an extension in the framework of DS theory with represented probability distributions assumed for each uncertain variables associated with belief structures, to study the impact of uncertainty in the input factors and their interactions on the considered quantifies of our interest.

This paper is organized as follows. We first provide the required background on peristalsis model, Dempster–Shafer theory, generalized polynomial chaos method, and sensitivity analysis in the framework of probability theory in Sect. 2. Then we specify the uncertain input parameters associated with mathematical representations and the considered quantities of interest from peristalsis model in the problem setup in Sect. 3. The numerical technique for mixed aleatory and epistemic uncertainty propagation and the exploratory sensitivity analysis in DS theory are provided in detail in Sect. 4. In Sect. 5, we apply the numerical technique to quantify the mixed types of uncertainty in the peristalsis models and analyze the sensitivity of flow characteristics and energetic costs with respect to uncertain input factors.

# 2 Background

In this section, we will provide the required background: peristalsis as the model system, the computational model of peristalsis, the basics of DS theory, generalized polynomial chaos, and sensitivity analysis.

#### 2.1 Peristalsis as the model system

A variety of systems in animals drive flow with valveless, tubular pumps (Griffiths et al. 1987; Gashev 2002; Xavier-Neto et al. 2010). Circulatory flow is driven by tubular, valveless pumps in many chordates, including tunicates and embryonic vertebrate hearts (Männer et al. 2010; Waldrop and Miller 2016; Battista et al. 2017a; Baird et al.



2015; Kozlovsky et al. 2016), providing important transport of oxygen, nutrients, and waste. In embryonic hearts, the physical forces involved in flow generated by tubular hearts partially controls the development of all organs (Jones et al. 2004).

Many of these valveless, tubular pumps use peristalsis to drive fluid flow. Peristalsis is a radial contraction of the walls of the tube which propagates down the length of the tube. Fluid within the system is driven in the same direction as the propagation of this wave. Although the system seems simple, the flow produced by a peristalsis-driven system depends non-linearly on several features: length and width of the pumping region, the closure of the tube's radius during pumping (compression ratio), the frequency of compressions traveling down the tube, and the overall scale (size) of the system (Waldrop and Miller 2016; Waldrop et al. 2020k). As a further complication, the relative importance of any of these features changes with the performance metric used for flow produced by the tube (e.g., mean flow speed or energetic cost of driving a unit of fluid through the circulatory system) (Waldrop et al. 2020k).

Many models have been used to approximate peristaltic flow to learn more about how these systems work in a biological context, including analytical and computational models (Pozrikidis 1987; Jaffrin and Shapiro 1971; Fung and Yih 1968; Shapiro et al. 1969). Analytical models typically make assumptions that limit the more direct application of their results to biological systems that employ peristalsis (Waldrop and Miller 2016). Recently, CFD models have been used to explore and clarify the mechanisms of pumping for vertebrate embryonic hearts, the presence of trabeculae, and the presence of blood cells (Waldrop and Miller 2016; Baird et al. 2014, 2015; Kozlovsky et al. 2016; Taber 2001; Taber et al. 2006; Battista et al. 2017a, b).

#### 2.2 Computational model of peristalsis

The computational models of closed-racetrack peristalsis are fully described in the following works: (Waldrop and Miller 2016; Waldrop et al. 2020k). For the self-completeness of current work, we provide the summarized equations here.

#### **Immersed Boundary Method**

The computational models were implemented using the immersed boundary method (IBM). IBM couples the movement of fluid with the movement of flexible boundaries moving either freely or with preferred motion. This model studied here was implemented in an open-source, parallelized version of the IBM called Immersed Boundary with Adaptive Mesh Refinement (IBAMR) (Griffith 2014). IBAMR is a C++ library that allows for direct, numerical simulation of the Navier–Stokes equations of fluid flow on a Eulerian grid that incorporates adaptive mesh refinement. Thereby, the Eulerian grid is larger (less resolved) farther away from areas of high vorticity and movement and more resolved closer to these areas in an effort to save computational resources.

The racetrack-shaped circulatory system consisted of two rigid boundaries tethered to fixed target points with an inner lumen, two straight sections connected by two curved regions, and a moving elastic region at the bottom of the racetrack, representing the heart tube that moved with a preferred motion. The racetrack design is consistent



13 Page 6 of 33 Y. He et al.

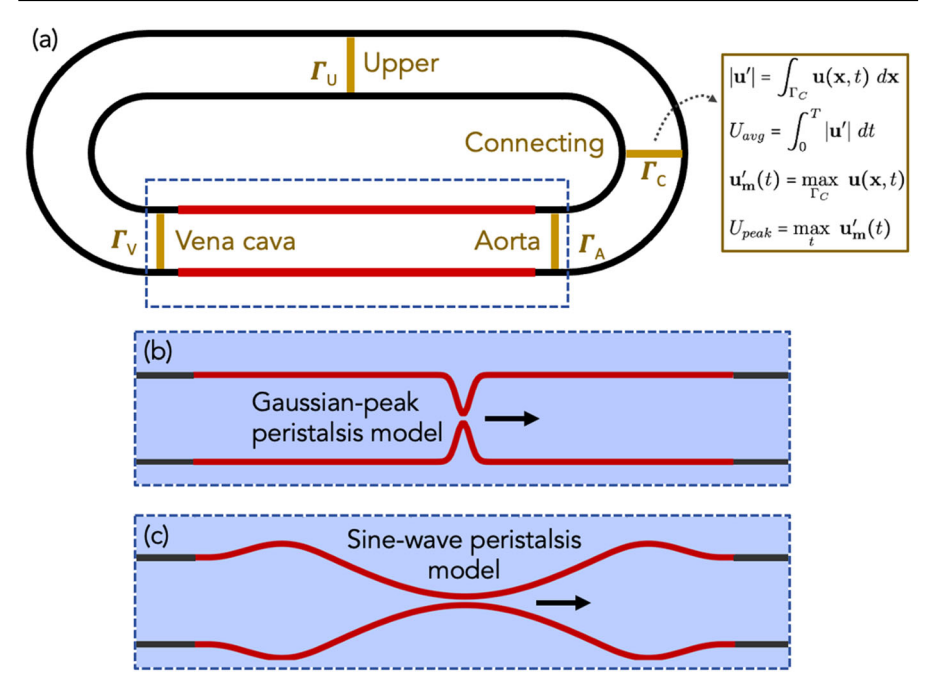


Fig. 1 a A cartoon schematic of the circulatory system, highlighting where flow data is analyzed. b Illustrations showing the  $\bf b$  Gaussian-wave and  $\bf c$  sine-wave peristalsis models

with past designs, thereby streamlining comparisons to previous studies (Jung and Peskin 2001; Lee et al. 2012; Baird et al. 2014; Waldrop and Miller 2016; Waldrop et al. 2020k).

The elastic region of the circulatory system had a 4:1 length:diameter ratio and created the motion to drive fluid through the circulatory system. The inner 3/4 of the elastic-tube length consisted of points tethered to target points. The movement of these tether points drove the preferred peristaltic motion according to the chosen waveform (either a sine wave or Gaussian-peak wave). The force equation adopted to drive peristalsis in the model is:

$$\mathbf{f}(r,t) = k_{targ}(\mathbf{Y}(r,t) - \mathbf{X}(r,t)) \tag{1}$$

where  $\mathbf{X}(r,t)$  and  $\mathbf{Y}(r,t)$  are the actual and preferred positions of the boundary, respectively. By differing the preferred motion of the boundary, we consider the following two different models of peristalsis, see Fig. 1 for an illustration of circulatory system as well as both peristalsis models.

#### Opposing sine-wave peristalsis model

The sine-wave model defines the motion of the boundary as two opposing sine waves:

$$y_{top,bot} = R_{top,bot} \pm A \sin(2\pi f t + 2\pi c x_t), \tag{2}$$



where f is the compression frequency, c is the compression-wave speed (held constant throughout the study at a non-dimensional speed of 3.0), A is the amplitude of the contraction, and  $x_t$  is the horizontal distance from the beginning of the prescribed motion section. The compression ratio (CR) gives the ratio of occlusion of the tube and is equal to 2A. The peristaltic waves created by Eq. 2 drives fluid flow counterclockwise in the lumen of the racetrack. The stiffness of the boundary and target points  $(k_{targ} = 30.0)$  resulted in little independent motion in the elastic region of the tube.

#### Opposing Gaussian-peak peristalsis model

Mixed uncertainty analysis on pumping by peristaltic...

The pinch model defines the motion of the boundary as two sharp, Gaussian peaks, with the remainder of the boundary remaining very flexible ( $k_{targ} = 0.7$ ) to allow for elastic interactions between the heart tube and its internal fluid. For the points within the region of the Gaussian wave, the target point stiffness was chosen to be extremely stiff ( $k_{targ} = 2500$ ) such that the target points matched closely to the prescribed waveform. The equation that governs the waveform is:

$$y_{top,bot} = R_{top,bot} \pm A \exp((-0.5(x_t - \gamma)/\sigma)^2), \tag{3}$$

where  $\gamma$  is the position of the pinch on the x-axis of the center of the tube and  $\sigma$  is the width of the pinch. The pinch was driven by altering  $\gamma$  depending on the time step of the simulation.

Both pumping models drive fluid through the circulatory system: a closure of the tube restricts flow through that region of the tube while simultaneously moving down the tube. However, each pumping model does so in a different way. The opposing sinewave model dictates a preferred motion along nearly every point on the tube while the Gaussian-peak model assigns preferred motion to only the opposing peaks, allowing the rest of the tube to flex to accommodate the displaced volume of the peaks. In terms of the animal, the Gaussian-peak model is closer to the kinematics of the heart, where contraction of the myocardium is limited to the compression point and the rest of the myocardium freely flexes to accommodate locally displaced fluid.

#### 2.3 Basics of DS theory

Let  $\xi \in Z$  be an input variable of a system, the value of which is unknown due to incomplete knowledge. We consider the following proposition "the true value of  $\xi$  is in A ( $A \subset Z$ )", and adopt belief functions Bel in DS theory to represent the strength of evidence supporting this proposition A. A belief function is defined as follows.

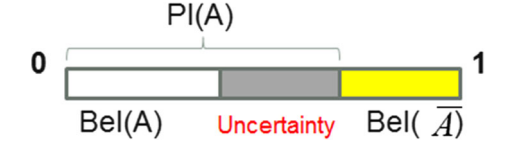
**Definition 1** A belief function assigns a number in [0, 1] to an element  $A \in 2^Z$  (Z is the universal set and  $2^{Z}$  is its power set), satisfying:

$$Bel(\emptyset) = 0,$$
  $Bel(Z) = 1,$   
 $Bel(\bigcup_{i=1}^{k} A_i) \ge \sum_{\emptyset \ne I \subseteq \{1,...,k\}} (-1)^{|I|+1} Bel(\bigcap_{i \in I} A_i), \text{ for } k \ge 2, A_1, ..., A_k \in 2^Z.$ 



13 Page 8 of 33 Y. He et al.

**Fig. 2** Belief Bel(A) and plausibility Pl(A)



Note that unlike probability density functions, belief functions do not have constraint of additivity. This relaxation makes them more suitable to represent epistemic uncertainty. Specifically,  $Bel(A) + Bel(\overline{A}) \le 1$ , where  $\overline{A}$  is the complement of A. When the summation is less than one, the remaining part (i.e.,  $1 - Bel(A) - Bel(\overline{A})$ ) can not be specified between supporting A or  $\overline{A}$  due to lack of information, therefore, goes to universal set Z, representing part of the epistemic uncertainty (see Fig. 2).

Adding this uncertain part to Bel(A), the maximum possible strength of evidence supporting a proposition A, denoted as Pl(A) is obtained. This function  $Pl: 2^Z \rightarrow [0, 1]$  is called plausibility function, defined as  $Pl(A) = 1 - Bel(\overline{A})$ .

Both belief and plausibility can also be defined as

$$Bel(A) = \sum_{B \subseteq A} m(B), \qquad Pl(A) = \sum_{B \cap A \neq \emptyset} m(B),$$
 (4)

where the basic belief assignment (BBA)  $m: 2^Z \to [0, 1]$ , also called m-function (we use BBA and m-function interchangeably in this work), assigns a number between 0 and 1 (called mass or belief mass) to an element  $A \in 2^Z$ , satisfying:

$$m(\emptyset) = 0, \qquad \sum_{A \subseteq Z} m(A) = 1.$$
 (5)

The element A with nonzero mass (i.e.,  $m(A) \neq 0$ ) is called a focal element. We assume the number of focal elements is finite in the current work.

The m-function can be interpreted with the concept of random sets (i.e., set-valued random variables) (Dubois and Prade 1991; Denaeux 2009; Tonon et al. 1991; Goodman and Nguyen 1985; Nguyen 1978) as follows. Let Z denote a non-empty set, let S be a finite family of distinct non-empty subsets of Z and  $\tilde{m}$  be a mapping  $S \to [0, 1]$  such that  $\sum_{A \in S} \tilde{m}(A) = 1$ , then the pair  $(S, \tilde{m})$  is a finite support random set on Z. The set S is equivalent to the collection of the focal elements of a belief function, and  $\tilde{m}(A)$ , which can be viewed as the probability of A, is equivalent to the belief mass m(A) for all  $A \in S$  (Dubois and Prade 1991). The extension principle for random sets through a function is also defined in (Dubois and Prade 1991; Tonon et al. 1991). We state the definition in the language of DS theory as follows (He and Hussaini 2023).

**Definition 2** Let  $u = f(\xi)$  be a mapping from the domain  $Z \subset \mathbb{R}^{n_Z}$  to a domain U, and let m be the BBA associated with input variable  $\xi$ , where its focal elements are a finite number  $\tilde{n}$  of subdomains  $A_1, A_2, \ldots, A_{\tilde{n}}$  ( $A_i \subset Z$ ), i.e., for any  $A \subset Z$ ,

$$m_{\xi}(A) = \begin{cases} m_{\xi}(A_i), & \text{if } A = A_i, & i = 1, \dots \tilde{n}, \\ 0, & \text{otherwise,} \end{cases}$$
 (6)



then the BBA of the output u (denoted as  $m_u$ ) is defined as, for any  $B \subset U$ 

$$m_u(B) = \begin{cases} \sum_{i \in S} m_{\xi}(A_i), S = \{i | f(A_i) = B\}, & \text{if } S \neq \emptyset, \\ 0, & \text{otherwise.} \end{cases}$$
 (7)

Cumulative belief function (CBF) and cumulative plausibility function (CPF) in DS theory, which are analogous to the cumulative distribution function in probability theory, are defined as follows.

**Definition 3** Let *Bel* be a belief function in DS theory, then its cumulative belief function and cumulative plausibility function are Oberkampf et al. (2001), Yager (2004)

$$CBF(z) = Bel(\xi \in (-\infty, z]), \tag{8}$$

$$CPF(z) = Pl(\xi \in (-\infty, z]). \tag{9}$$

# 2.4 Generalized polynomial chaos

In this work, generalized polynomial chaos expansions will be constructed as computationally cheaper surrogates to approximate the statistics of quantities of our interest in the stochastic space. Here are the basics.

Let  $\boldsymbol{\xi} = \{\xi_1(\omega), \xi_2(\omega), \dots, \xi_n(\omega)\}: \Omega \to \Xi \subseteq \mathbb{R}^n$  denote a set of n uncorrelated random variables representing the uncertainty in the system, where  $\omega$  is defined in a probability space  $(\Omega, \mathcal{F}, \mathcal{P})$ :  $\Omega$  is sample space,  $\mathcal{F} \subset 2^{\Omega}$  is the  $\sigma$ -algebra and  $\mathcal{P}: \mathcal{F} \to [0, 1]$  is the probability measure. Let  $u(\boldsymbol{\xi}(\omega)) \in \mathbf{L}_2(\Omega, \mathcal{P})$  be any second-order random variables, i.e.,  $\langle u, u \rangle = \|u\|_{\Omega}^2 \langle \infty \rangle$ . Then u can be represented using gPC expansions (Cameron and Martin 1947; Ghanem and Spanos 1991; Wiener 1938):

$$u(\boldsymbol{\xi}(\omega)) = \sum_{i=0}^{\infty} \hat{u}_i \Phi_i(\boldsymbol{\xi}(\omega)), \tag{10}$$

where  $\hat{u}_i$ s are called gPC coefficients, which will be decided from specific simulations;  $\Phi_i$  are generalized polynomial chaos, which originate from Hermite polynomials corresponding to Gaussian distributed random inputs (Wiener 1938), then include different types of orthogonal polynomials in the Askey scheme corresponding to different types random variables (Xiu and Karniadakis 2003, 2002). In this work, we will adopt Legendre polynomials with uniformly distributed input parameters. The first few one-dimensional Legendre polynomials are:

$$\Phi_0(\xi) = 1, \quad \Phi_1(\xi) = \xi, \quad \Phi_2(\xi) = \frac{1}{2}(3\xi^2 - 1), \dots$$

and high-dimensional Legendre polynomials can be obtained by taking the product of univariate Legendre polynomials. Further details can be found in Xiu (2010).



13 Page 10 of 33 Y. He et al.

For the purposes of numerical computing, truncated gPC expansion up to polynomial order p is used to approximate the exact output  $u(\xi(\omega))$ 

$$u_p(\boldsymbol{\xi}(\omega)) = \sum_{i=0}^{N-1} u_i \Phi_i(\boldsymbol{\xi}(\omega)), \tag{11}$$

where  $N = \frac{(n+p)!}{n!p!}$  is the number of terms. The gPC coefficients  $u_i$  can be calculated by projecting u on each basis (with inner product) due to the orthogonality of polynomial functions. Here is the formula:

$$u_{i} = \frac{\langle u, \Phi_{i} \rangle}{\langle \Phi_{i}, \Phi_{i} \rangle} = \frac{1}{E[\Phi_{i}^{2}]} \int_{\Xi} u(\xi) \Phi_{i}(\xi) \eta(\xi) d\xi, \tag{12}$$

where  $\eta(\xi)$  is the probability distribution of the variable  $\xi$ . This projection method leads to the best approximation in the weighted L2 norm (Xiu 2010). However, the accuracy may be strongly influenced by the limited computational resources for numerical integration especially over high-dimensional space. Alternatively, the gPC coefficients can also be estimated by simply solving a Least Squares problem using a dataset—the quantities of interest extracted from a number of full simulations for the corresponding inputs  $\{\xi^{(j)}, u^{(j)}\}_{j=1}^{M}$ . The Least Squares problem for the solution  $u = [u_0, u_2, \ldots, u_{N-1}]$  is stated as

$$\mathbf{u} = \arg\min_{\tilde{\mathbf{u}}} \left\| \sum_{i=0}^{N-1} \tilde{u}_i \Phi_i(\xi) - u(\xi) \right\|_2, \tag{13}$$

where  $\tilde{\boldsymbol{u}} = [\tilde{u}_0, \tilde{u}_1, \dots, \tilde{u}_N]$  denotes an arbitrary gPC coefficient vector that converges to the desired coefficient vector  $\boldsymbol{u}$  through the minimization.

#### 2.5 Sensitivity analysis

With the constructed gPC expansions as computationally cheaper surrogates, one can further analyze the relations between uncertain inputs and outputs efficiently using sensitivity analysis. In this section, we introduce a variance-based sensitivity analysis method—Sobol' indices (SI), to measure the global sensitivity of flow characteristics and energetic costs (driving the flow) with respect to the uncertainty in input parameters. The Sobol' indices can help to rank the "importance" of the uncertain input parameters by comparing the impact of their variation on the considered quantities of our interest. They are calculated based on the analysis of variance (ANOVA) decomposition of a function  $u(\xi)$  as (Sobol' 1993, 2001; Sudret 2008; Sobol' and Kucherenko 2005):

$$u(\boldsymbol{\xi}) = u_0 + \sum_{i} u_i(\xi_i) + \sum_{i < j} u_{ij}(\xi_i, \xi_j) + \dots + u_{1,\dots,n}(\xi_1, \xi_2, \dots, \xi_n).$$
 (14)



where

$$\int u(\xi) d\xi = u_0,$$

$$\int u(\xi) \Pi_{k \neq i} d\xi_k = u_0 + u_i(\xi_i),$$

$$\int u(\xi) \Pi_{k \neq i,j} d\xi_k = u_0 + u_i(\xi_i) + u_j(\xi_j) + u_{i,j}(\xi_i, \xi_j),$$

and so on.

The Sobol' indices are the partial variances (attributed to one or more uncertain parameter interactions  $\{\xi_{i_1}, \xi_{i_2}, \dots, \xi_{i_r}\}$ ) normalized by the overall model variance. The partial variance  $(V_{i_1,i_2,\dots,i_r})$  and total variance (V) can be expressed in the following manner:

$$V_{i_1,i_2,\dots,i_r} = \int u_{i_1,i_2,\dots,i_r}^2 d\xi_{i_1} \dots d\xi_{i_r},$$

$$V = \int u^2(\xi) d\xi - u_0^2 = \sum_{r=1}^n \sum_{i_1 < \dots < i_r}^n V_{i_1,i_2,\dots,i_r}.$$

Therefore, the Sobol' indices are defined as:

$$S_{i_1,i_2,...,i_r} = V_{i_1,i_2,...,i_r}/V.$$
 (15)

Numerically, Monte Carlo sampling methods can be used to estimate the Sobol' indices. Below we describe the sampling procedure from Sobol' work (Sobol' 2001). Denote  $y = (\xi_{i_1}, \xi_{i_2}, \dots, \xi_{i_r})$ ,  $I = (i_1, i_2, \dots, i_r)$ , the variance corresponding to the set y is the summation of the variance associated with all the subset of y as

$$V_{\mathbf{y}} = \sum_{s=1}^{r} \sum_{(k_1 < \dots < k_s) \in I} V_{k_1, \dots, k_s}.$$

Based on the following equality from Sobol' (2001),

$$V_{\mathbf{y}} = \int u(\boldsymbol{\xi})u(\mathbf{y}, z')d\boldsymbol{\xi}dz' - u_0^2,$$

the quantity  $V_y$  can be estimated using the following MC method. First, we generate two independent set of N random samples for  $\xi$  based on its specified probability density function, denoted as  $x = (\tau, \zeta)$  and  $x' = (\tau', \zeta')$ , where  $\tau$  are the samples corresponding to set of variables y. Then we produce the estimations using the following formulas:

$$u_0 \approx \frac{1}{N} \sum_{j=1}^{N} u(x_j),$$



13 Page 12 of 33 Y. He et al.

$$V \approx \frac{1}{N} \sum_{j=1}^{N} u^{2}(x_{j}) - u_{0}^{2},$$

$$V_{y} \approx \frac{1}{N} \sum_{j=1}^{N} u(x_{j}) u(\tau_{j}, \zeta_{j}') - u_{0}^{2}.$$

Note: In the probabilistic framework where the probability density function is specified for each random input, Sobol' indices can be estimated more efficiently using gPC coefficients directly (Sudret 2008). However, in the non-probabilistic setup as in our current work with uncertain but not random inputs, gPC is constructed to serve as computational cheaper surrogate.

# 3 Problem setup

In this section, we specify the uncertain input parameters and the considered quantities of interest from peristalsis model.

# 3.1 Flow characteristics and energetic cost

In order to study the fluid motion produced by the pumping model simulations, several non-dimensional qualities of interest from the fluid flow and pressure were calculated for each simulation. Raw data from the simulation was imported into VisIt 3.3 (Childs et al. 2012) and python scripts (Python 2) were used to automate calculations across the Eulerian grid. Results from these calculations were then imported into *R* v4.0.2 (R Core Team 2021) for calculation of simulation-wide performance values. All code used to calculate these values can be found in the Github repository: https://github.com/lindsaywaldrop/peri-gPC-git. All positive flow motion indicates counter-clockwise movement in the racetrack, the same direction as the traveling peristaltic waves. All values presented are dimensionless.

The magnitude of the dimensionless fluid velocity was recorded in IBAMR at each time-reporting step in the simulation (see Fig. 3 for examples of flow profiles of both pumping models). These values were then spatially averaged in VisIt across the diameter of the tube in four areas (immediately upstream of the heart tube, immediately downstream of the heart tube, in the connecting U perpendicular to the contraction wave, and in the middle of the still circulatory system parallel to the contraction wave, see Figs. 1 and 3) to find the mean speeds, ( $|\mathbf{u}'|$ ). The mean speeds ( $|\mathbf{u}'|$ ) were then temporally averaged to find the average flow speed across each simulation ( $U_{avg}$ ). At each reporting time step, the maximum value of flow speed ( $\mathbf{u}'_{m}$ ) was taken in VisIt and the maximum of these values represents peak flow speed ( $U_{peak}$ ).

Each reporting time step of the simulation also yielded non-dimensional pressure. These were spatially averaged at each time step near the immediate upstream and immediate downstream of the heart tube. For each simulation, both positions were averaged temporally to find  $p_{in}$  and  $p_{out}$ , respectively. The difference of these values represents  $\Delta P$ .



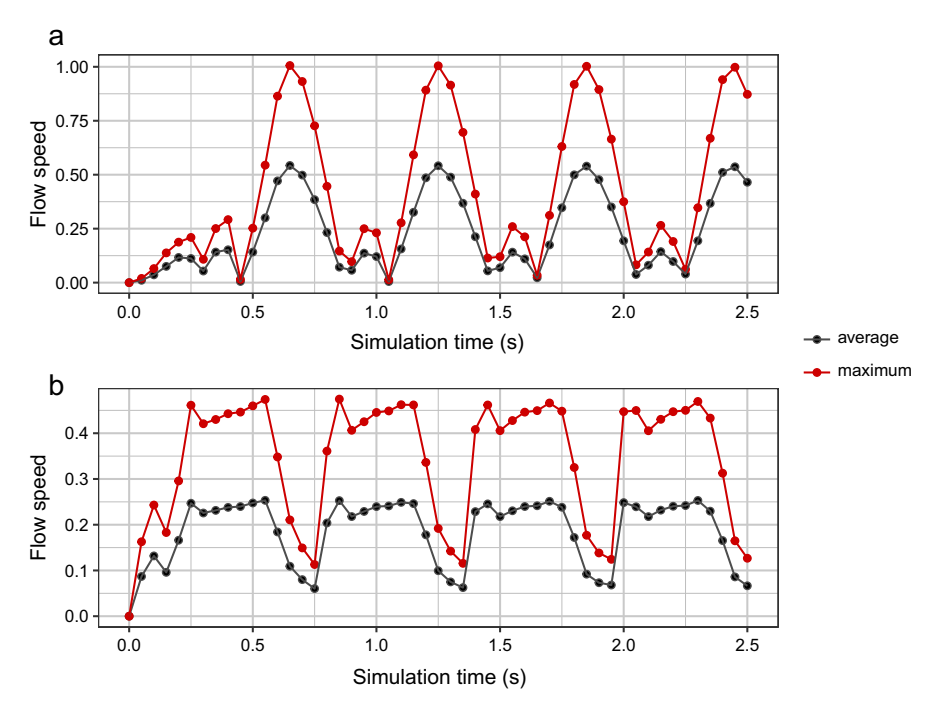


Fig. 3 Flow dynamics in the circulatory system produced by **a** sine-wave and **b** Gaussian-peak peristalsis models for a simulation where  $f = 1.68\,\mathrm{Hz}$ , CR=0.888, and Wo=1.216. Dark grey points lines represent the flow speed in the upper connecting tube ( $\Gamma_U$  in Fig. 1a) averaged across its diameter. Red points and lines represent the maximum flow value of the averaged profile at  $\Gamma_U$  for that time step

Volume flow rate was calculated with the velocity provide perpendicular to axis of the heart tube for each simulation, analyzed in VisIt. Each value at each reporting time step was used to calculate a concentric ring of fluid that passed through the tube during that time step based on the velocity at that position in the tube. These rings were summed to find the volume flow rate at that time step, then these values were averaged temporally to find the average volume flow rate of the simulation, Q.

The cost of transport (COT) was computed using the mean flow speed, the average force magnitude at each of the Langrangian points of the tube driving motion, and the contraction velocity of the tube. For additional details of this calculation, see Waldrop and Miller (2016), Waldrop et al. (2020k).

#### 3.2 Uncertain input parameters

As stated in our previous work (Waldrop et al. 2020k), based on potential effects on functional performance and the ability of the parameter to vary in animals with valveless, tubular hearts, and their representation in the model, three parameters were selected: Compression ratio (CR), which measures percent occlusion of the tube during a compression event. Compression frequency (f), which reflects the number of



13 Page 14 of 33 Y. He et al.

compression events per unit time, and Womersley number (Wo), a ratio of inertia over viscous forces in flow, which reflects roughly the fluid regime of many tubular hearts.

Each of these parameters affects the system in different ways. CR serves to build pressure against the resistive circulatory system and drive fluid forward. f determines the time elapsing between beats. We describes the inertial components of flow to viscosity, determining how much force is needed to overcome the viscous resistance of the circulatory system to flow.

The value ranges for each parameter were gathered from both observations and published values of hearts for tunicates (Kalk 1970; Heron 1973; Bone et al. 1997; Waldrop and Miller 2015; Konrad 2016), the mosquito *Anopheles gambiae* (Glenn et al. 2010), an embryonic fish *Danio rerio* (Forouhar et al. 2006), and embryonic chickens (Hu and Clark 1989; Midgett et al. 2014).

Based on these values, we make the following assumptions regarding the further distributions of these three parameters inside the whole ranges: CR varies from 0.4 (reduction of 40% of the tube's diameter) to 0.95 (reduction of 95% of the tube's diameter); f varies between 0.5 and 2.0 beats per second; and Wo varies between 0.1 and 10. Rigorous construction of belief functions from data is out of the scope of the current work.

- 1. The frequency f is assumed to be stochastic and uniformly distributed over the range [0.5, 2].
- 2. The Womersley number Wo is a non-probabilistic uncertain variable associated with a BBA (the *m*-function) as

$$m_{\text{Wo}}(D_{1,1}) = 0.4$$
;  $m_{\text{Wo}}(D_{1,2}) = 0.4$ ;  $m_{\text{Wo}}(D_{1,3}) = 0.2$ ,

where the focal elements  $D_i$ s are overlapped intervals

$$D_{1,1} = [0.1, 1); D_{1,2} = [1, 10]; D_{1,3} = [0.1, 10].$$

The compression ratio CR is another non-probabilistic uncertain variable associated with a BBA as

$$m_{\rm CR}(D_{2,1}) = 0.3; m_{\rm CR}(D_{2,2}) = 0.2; m_{\rm CR}(D_{2,3}) = 0.3; m_{\rm CR}(D_{2,4}) = 0.2,$$

where the focal elements  $D_i$ s are overlapped intervals

$$D_{2,1} = [0.4, 0.5); D_{2,2} = [0.5, 0.8); D_{2,3} = [0.8, 0.95]; D_{2,4} = [0.4, 0.95].$$

#### 4 Methods

In this section, we introduce the numerical strategy for mixed uncertainty propagation in the computational model of peristalsis, and the calculation of Sobol' indices in the framework of Dempster–Shafer theory.



#### 4.1 Mixed uncertainty propagation

As assumed in the problem setup, both epistemic and aleatory uncertainties exist in the system. Furthermore, the epistemic uncertainty is characterized by the uncertain non-probabilistic variables  $\xi = \{\text{Wo, CR}\} \in Z \text{ associated with BBAs, while the aleatory uncertainty is characterized by random variable <math>f \in Y \text{ associated with a uniform distribution.}$  The mixed types of uncertainty are propagated through the system, and the goal is to mathematically represent the uncertainty in the output (using flow volume rate Q as an example)  $Q(\xi, f) \in Z \times Y$ .

Dealing with aleatory uncertainty using Monte Carlo simulation. With the available probability density function (denoted as  $\eta(f)$ ) for the random variable f, one can calculate the statistics of output Q over the stochastic space Y, such as its expectation (denoted as E) and standard deviation (denoted as S)

$$E(\xi) = E[Q(\xi, f)|\xi] = \int_{Y} Q(\xi, f)\eta(f)df, \quad \xi \in Z.$$
 (16)

$$S(\xi) = \sqrt{E[Q^2(\xi, f)|\xi] - E^2(\xi)} = \sqrt{\int_Y (Q(\xi, f) - E(\xi))^2 \eta(f) df}.$$
 (17)

Numerically, we approximate the integration using Monte Carlo simulations as

$$E(\xi) \approx \frac{1}{M} \sum_{i=1}^{M} Q(\xi, f^{(i)}), \quad S(\xi) \approx \sqrt{\frac{1}{M} \sum_{i=1}^{M} (Q(\xi, f^{(i)}) - E(\xi))^2},$$
 (18)

where  $f^{(i)}$  (i = 1, ..., M) are the samples of random variable f drawn based on its uniform distribution.

Due to the mixed types of uncertainty, such statistics (e.g.,  $E(\xi)$ ,  $S(\xi)$ ) are not deterministic, but functions of the non-probabilistic variable  $\xi$  over the domain Z. Since a BBA is associated with the input variable  $\xi$ , the goal then becomes to obtain a BBA for the statistics of model output efficiently.

Dealing with epistemic uncertainty using DS theory. Consider the statistics (with  $E(\xi)$  as an example), where  $\xi = \{\text{Wo}, \text{CR}\} \in Z$ . Uncertainty propagation using DS theory is to find the BBA (m-function) for the output E given the BBAs for each elements of input vector  $\xi$ .

We first construct two-dimensional belief structure for  $\xi$  by taking the Cartesian product over both the directions of  $\xi$ . The universal set will be  $Z=Z_1\times Z_2$ . The focal elements are  $D_k=D_{1k_1}\times D_{2k_2}$  for  $1\leq k\leq 3\times 4$ , where  $D_k$  is a two-dimensional hypercube. The focal elements are visualized in the left plot of Fig. 4. The mass of each focal element is  $m_{\xi}(D_k)=m_1(D_{1k_1})m_2(D_{2k_2})$ . For example, let  $D_k=[0.1,1]\times[0.8,0.95]$  as in Fig. 4, then  $m(D_k)=m_{\text{Wo}}([0.1,1])m_{\text{CR}}([0.80.95])=0.12$ . The construction can be easily extended to higher-dimensional belief structure as described in He and Hussaini (2023).

The uncertainty in  $\xi$ , represented by the two-dimensional BBA, is propagated through the peristalsis heart pumping system and accumulated in the uncertainty of



13 Page 16 of 33 Y. He et al.

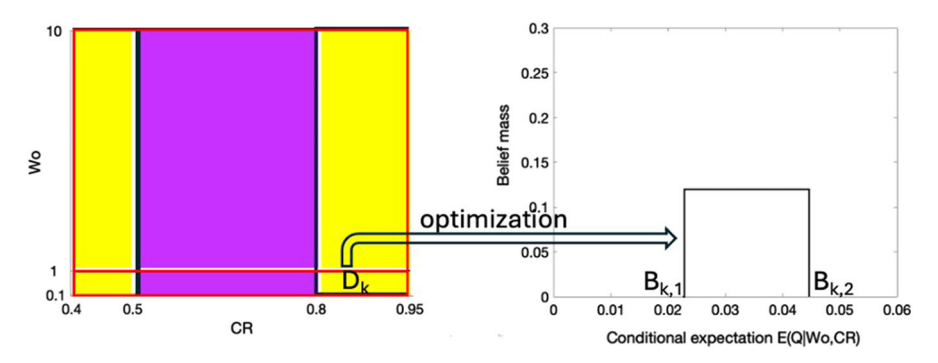


Fig. 4 Illustration of epistemic uncertainty propagation

the output flow volume  $Q(\xi)$ , and consequently its statistics E. The BBA of the output E (based on Def. 2) can be used to represent the uncertainty in E. For the purpose of numerical computation, we construct the BBA by first solving a pair of optimization problems in each hypercube  $D_k$ .

$$B_{k,1} = \min_{\xi \in D_k} E(\xi), \qquad B_{k,2} = \max_{\xi \in D_k} E(\xi).$$

Under the assumption that the output flow volume Q is continuous in Z, the interval  $B_k = [B_{k,1}, B_{k,2}]$  becomes one focal element of the BBA for E with belief mass  $m_{\xi}(D_k)$ . For example, as shown in Fig. 4, two optimizations of  $E(Q|\xi)$  for pinch model over the domain  $D_k$  are carried out, and the interval from  $B_{k,1} = 0.0228$  to  $B_{k,2} = 0.0441$  forms one output focal element with belief mass 0.12. As stated in He and Hussaini (2023), the BBA of the output E should have the same number of focal elements as the BBA of  $\xi$  unless there are more than one hypercubes corresponding to the same focal element for E.

#### 4.2 Physics constrained gPC for surrogates

The introduced approach can be computationally expensive due to the large number of simulation runs, required by the evaluation of statistics and the optimization algorithm. To reduce the computational cost, we construct a computationally cheaper surrogate (e.g.,  $Q_{\rm gPC}$ ) using gPC expansion to approximate the full simulation Q so that the uncertainty in the model output can be represented more efficiently.

$$Q_{\text{gPC}}(\xi) = \sum_{i=0}^{N-1} q_i \Phi_i(\xi).$$
 (19)

The adoption of efficient gPC method can improve our ability to study complex CFD models.

In this work, we run M=681 full CFD simulations and extract a set of quantities of interest corresponding to the inputs  $\xi$ . With the data set, we obtain the gPC coefficient



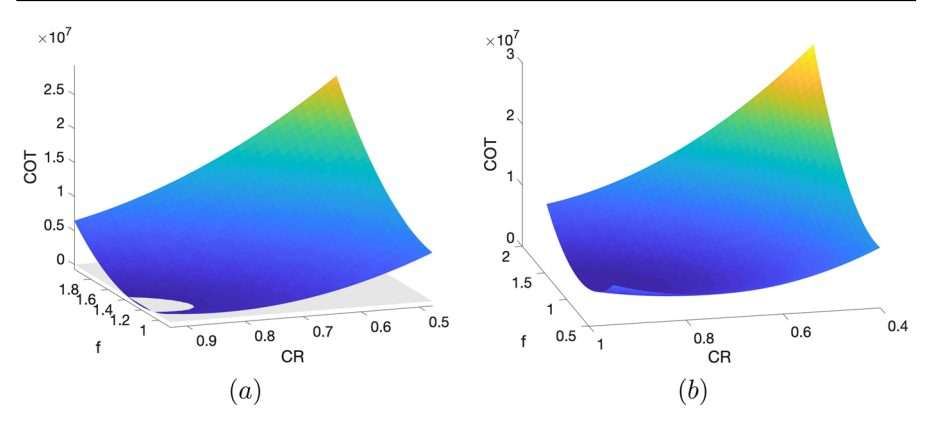


Fig. 5 Comparison of gPC expansion for COT with respect to CR and f a without positivity constraint, and  $\mathbf{b}$  with positivity constraint

using least squares method as in Eqn. 13. However, the obtained surrogates  $Q_{\rm gPC}$  purely from data set (simulation outputs) may not satisfy some important physical properties of the underlying problem, such as the conservation principles expressed with partial differential equations in fluid dynamics, other physical or biological constraints present in the system, or positivity of some quantities of interest. To produce physically more meaningful surrogates from data-driven approaches, we introduce the physical constraints into the process of surrogate construction. Specifically, we enforce positivity for the flow volume Q in the gPC expansion. Since it is challenging to enforce the constraints over the entire space (Swiler et al. 2020), we relax the global requirement and enforce the constraints on the surrogate prediction  $Q_{\rm gPC}(\xi)$  from gPC over a finite set of "virtual" points  $\xi_i^c$ . Then we can minimize the  $L_2$  norm of the difference between gPC expansion prediction  $Q_{\rm gPC}^{(j)}$  and deterministic simulation output  $Q^{(j)}$  ( $j=1,\ldots,M$ ) subject to the physical constraints with respect to the gPC coefficients  $q=\{q_0,\ldots,q_{N-1}\}$ .

$$\min_{\mathbf{q}} \|Q_{\text{gPC}}(\xi, \mathbf{q}) - Q(\xi)\|_{2}, 
\text{s.t. } Q_{\text{gPC}}(\xi_{i}^{c}, \mathbf{q}) > 0, \quad i = 1, \dots, n_{c}$$
(20)

The constructed surrogate  $Q_{\rm gPC}$  can serve as efficient yet quantitative regimes within input parameter spaces, and further be used for model prediction and uncertainty analysis.

For the purpose of illustration, we provide an example of comparison between gPC expansion with positivity constraint and the one without the constraint. Specifically, we consider COT from sine wave model as current QoI and enforce the positivity constraint during the construction of gPC expansion over three dimensions. For a better visualization, we have plotted the surfaces with varying CR, f and a fixed Wo= 5.05 in Fig. 5. One can obverse that gPC expansion constructed from data points only results in negative COT (below the grey surface with zero values in Fig. 5a), while gPC expansion with physics constraints satisfies the desired property.



13 Page 18 of 33 Y. He et al.

# 4.3 Exploratory sensitivity analysis in the framework of DS theory

The variance-based global sensitivity analysis is introduced in the framework of probability theory. To implement it in DS theory, there are a few challenges as stated in the work from Helton et al. (2006a): (i) How to specify the probability density function that are consistent with the belief structure, (ii) How to implement the analysis in a computationally practicable manner, and (iii) how to display the SA results. Regarding the first challenge, we adopt the exploratory approach from Helton et al. (2006a) to select three representative probability density functions: one distribution uniform over the range of each focal element (uniform), another one emphasizing the smaller values associated with each focal element (left quadratic), and the third one emphasizing the larger values associated with each focal elements (right quadratic). For example, over the j-th focal element  $[a_{i,j}, b_{i,j}]$  associated with uncertain variable  $\xi_i$ , the three distributions for uniform, left quadratic and right quadratic are provided here as  $d_{uij}$ ,  $d_{lij}$  and  $d_{rij}$ , respectively:

$$d_{uij}(\xi_i) = \frac{1}{(b_{i,j} - a_{i,j})}, \qquad d_{lij}(\xi_i) = \frac{3(b_{i,j} - \xi_i)^2}{(b_{i,j} - a_{i,j})^3}, \qquad d_{rij}(\xi_i) = \frac{3(\xi_i - a_{i,j})^2}{(b_{i,j} - a_{i,j})^3},$$

if  $\xi_i \in [a_{i,j}, b_{i,j}]$  and  $d_{uij}(\xi_i) = d_{lij}(\xi_i) = d_{rij}(\xi_i) = 0$  otherwise. In turn, the uniform, left quadratic and right quadratic distributions for  $\xi_i$  over the universal set  $[a_i, b_i]$  is given by

$$d_{ci}(\xi_i) = \sum_{i=1}^{C_i} m_i([a_{i,j}, b_{i,j}]) d_{cij}(\xi_i),$$

where c = u, l, r, and  $C_i$  is the number of focal elements for  $\xi_i$ .

To mitigate the second issue, we construct gPC approximation as surrogate over the whole domain. The computational cost mainly lies in the construction of gPC surrogate. The estimation of variances and consequently the estimation of Sobol' indices with constructed surrogate has relatively negligible computational cost. Regarding the third issue, similar as in Helton et al. (2006a), we plot a spectrum of sensitivity analysis results (carried out for each individual probability distribution) together instead of a single SA result.

# 5 Numerical examples

In this section, we mathematically represent the uncertainty in flow volume rate, cost of transport and work for both sine-wave and Gaussian-peak peristalsis models. In addition, the sensitivity of considered quantities of interest with respect to the uncertain inputs are analyzed and the Sobol' indices are provided.



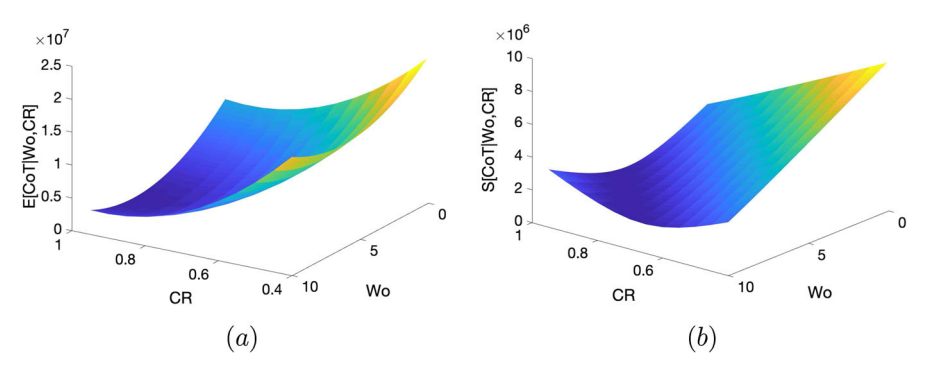


Fig. 6 Statistics surfaces of COT averaged over stochastic space: a mean surface, and b standard deviation surface

#### 5.1 Quantities with sine wave

#### 5.1.1 Surrogate surfaces

The introduced method is applied to quantify the mixed types of uncertainty in the output quantities of interest propagated from the uncertainty in inputs. In other words, the QoI statistics are obtained in stochastic space corresponding to aleatory uncertainty and then BBAs are constructed to represent the epistemic uncertainty in the conditional statistics value of the output QoI. To increase the computational efficiency, gPC method is adopted to construct a surrogate model as an approximation. Take the QoI COT from sine wave as an example, the two-dimensional gPC expansions of expectation and standard deviation (over stochastic space) with respect to the two non-probabilistic uncertain variable Wo and CR are provided in Fig. 6.

# 5.1.2 Uncertainty representation for COT

Using the constructed surrogate model with approximation order n=2, the BBA of the numerical conditional expectation  $m_{E(\text{COT})}$  is then constructed. As mentioned earlier, the m-function of the uncertain inputs have 12 focal elements associated with different degrees of belief mass. Therefore, the number of focal elements for  $m_{E(\text{COT})}$  will also be 12 and the belief masses will be the same as the ones of their corresponding input focal elements (optimization domains). The focal elements and the belief masses are:



13 Page 20 of 33 Y. He et al.

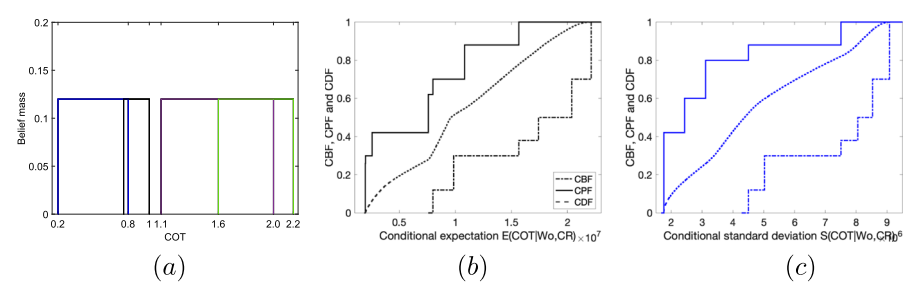


Fig. 7 Sine COT: **a** focal elements with the highest belief mass; **b** cumulative functions for the expectation, and **c** cumulative functions for the standard deviation

From the BBA, one can conclude that the expectation of the output solution will be inside the intervals  $B_1$ ,  $B_2$ ,  $B_7$  and  $B_8$  with maximum degree of belief 0.12 (see Fig. 7a), and no preference will be given to any more specific subsets of those intervals due to the mixed types of uncertainty. With obtained BBA  $m_{E_n}$ , the CBF and CPF are calculated and plotted in Fig. 7b, which bound the possible true cumulative distribution function (CDF) of the expectation of output E(COT|Wo, CR). For example, if it is assumed that Wo and CR are both random, and furthermore the distribution under each focal elements are uniform, the CDF can be constructed to represent the uncertainty in E(COT|Wo, CR) instead of CBF and CPF. As expected, the dashed curve (CDF) falls between the CBF and the CPF since the CDF with uniform distribution is a special case of all possible probability distributions consistent with the belief/plausibility structure. With CBF and CPF, one can make conclusions about the quantity E(COT). For example, if the proposition  $E(COT) \le 1.2$  is considered, one can conclude that probability of the proposition being true is bounded between 0.3 and 0.88. Similarly, the BBA of numerical conditional standard deviation  $m_{S_n}$  is also constructed, and the corresponding CBF/CPF are plotted in Fig. 7c, which bounds the CDF obtained under assumption of uniform distribution over each focal elements.

#### 5.1.3 Uncertainty representation for volume flow rate Q

We are also interested in the output volume flow rate. Again, the mixed types of uncertainty in Q is represented using the BBA of the conditional expectation E(Q|Wo, CR) and conditional standard deviation S(Q|Wo, CR). The CBF and CPF are then calculated from BBA and the figures (see Fig. 8) are provided here for a better visualization. From the curves of CBF and CPF, one can observe the lower and upper bounds of how



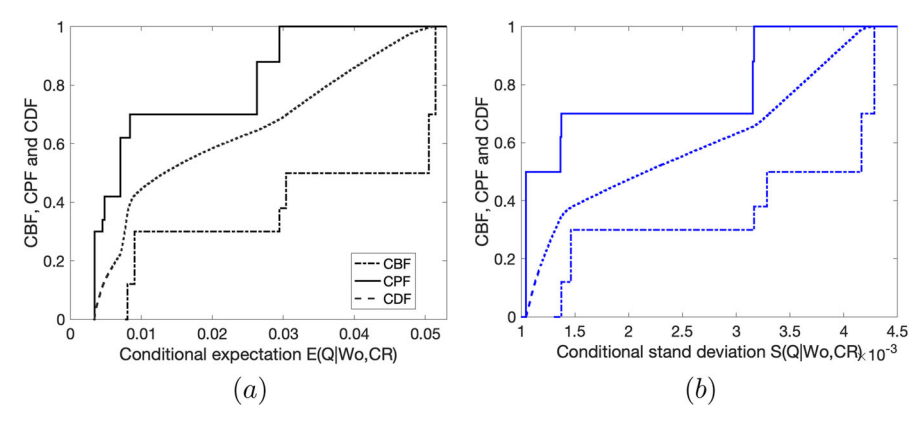


Fig. 8 CBF, CDF and CPF for statistics of Sine volume flow rate: a expectation, and b standard deviation

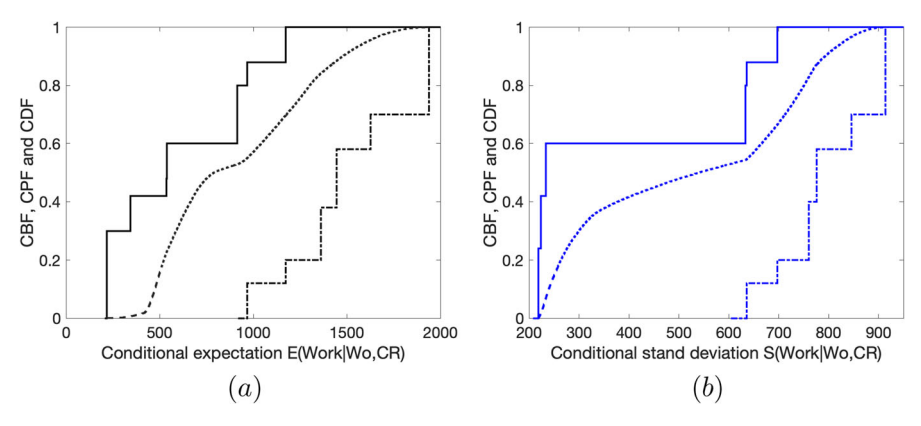


Fig. 9 CBF, CDF and CPF for statistics of Sine work: a expectation, and b standard deviation

likely that the conditional expectation and conditional standard deviation is below a fixed value. For example, the true probability of  $E(Q|\text{Wo},\text{CR}) \leq 0.02$  is bounded by 0.3 and 0.7, and the true probability of  $S(Q|\text{Wo},\text{CR}) \leq 0.0035$  would be bounded by 0.5 and 1. Similarly, one example of CDF (under the assumption that Wo and CR are uniform under focal elements) is provided for both expectation E(Q) and standard deviation S(Q), and plotted in Fig. 8. As expected, the CDFs are bounded by the corresponding CBFs and CPFs.

#### 5.1.4 Uncertainty representation for work

Work is another output quantity of our interest that we investigate the mixed types of uncertainty. Similarly, from the constructed BBA for conditional expectation E(work|Wo, CR) and conditional standard deviation S(work|Wo, CR), we calculate the corresponding CBF and CPF and plot the curves in Fig. 9. We also provide the same example of one CDF under the assumption of uniform distribution in each focal elements, which are bounded by the corresponding CBF and CPF as expected.



13 Page 22 of 33 Y. He et al.

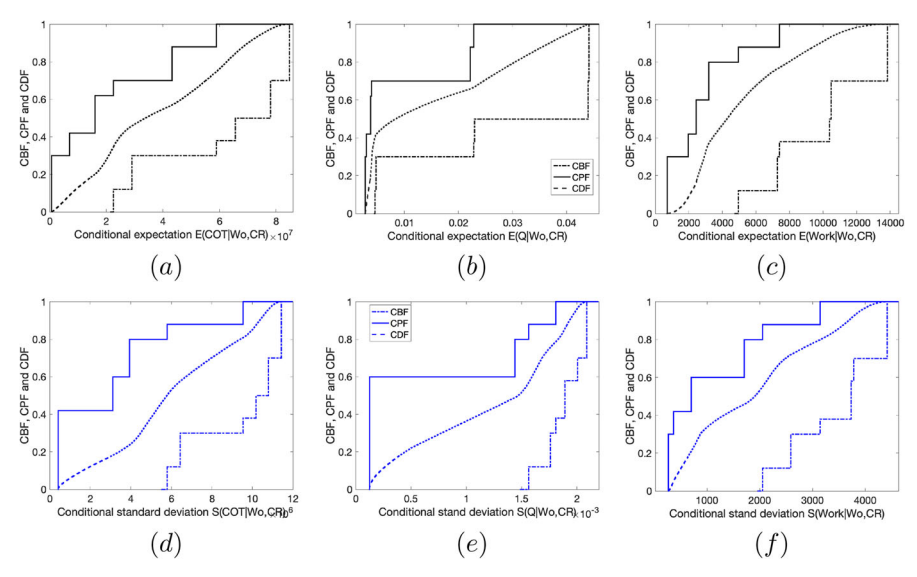


**Fig. 10** CBF, CDF and CPF for statistics of Pinch wave model: **a** expectation for COT pinch, **b** expectation for Q pinch, **c** expectation for work pinch, **d** standard deviation for COT pinch, **e** standard deviation for Q pinch, and **f** standard deviation for work pinch

# 5.2 Quantities with pinch wave

We also study the mixed types of uncertainties in the output of pinch model, where the motion of the boundary is defined as two sharp, Gaussian peaks. Similarly, we consider the cost of transport (COT), flow volume rate (Q) and the work.

The CBF and CPF (lower and upper bounds of possible true CDF) and one example of CDF (under the assumption of uniform distribution within each focal elements) are calculated for the conditional expectation and conditional standard deviation of the QoIs from the pinch model. The curves are plotted in Fig. 10. For the cost of transport, one can observe that  $P(E(\text{COT}|\text{Wo},\text{CR}) \leq 2.22e + 7)$  is below 0.62 for pinch wave model, compared to  $P(E(COT|Wo, CR) \le 2.22e + 7) = 1$  for sine wave model. For flow volume rate, the plot shows that the possible true probability of  $E(Q|W_0, CR) \le 0.01$  is bounded by 0.3 and 0.7 (for both sine wave and pinch model), and  $0.5 \le P(E(Q|W_0, CR) \le 0.03) \le 1$  for the pinch model (compared to  $0.38 \le P(E(Q|W_0, CR) \le 0.03) \le 1$  for the sine wave model). For work, we have  $0 \le P(E(\text{work}|\text{Wo}, \text{CR}) \le 1000) \le 0.3 \text{ (compare to } 0.12 \le P(E(\text{work}|\text{Wo}, \text{CR}) \le 1000)$  $1000 \le 0.88$  from sine wave model) and  $P(E(\text{work}|\text{Wo}, \text{CR}) \le 14000) = 1$  (compare to  $0.38 \le P(E(\text{work}|\text{Wo}, \text{CR}) \le 14000) \le 1$  from sine wave model). Similarly, the bounds of the probability of conditional standard deviation of QoIs less than any fixed value can also be read from the bottom row of Fig. 10. If one is interested in a fixed probability number instead of the bounds, under the assumption of a special case (e.g., uniform distribution within focal elements), the probability of conditional statistics less than a fixed value can be found from the middle dashed curves in each plot.



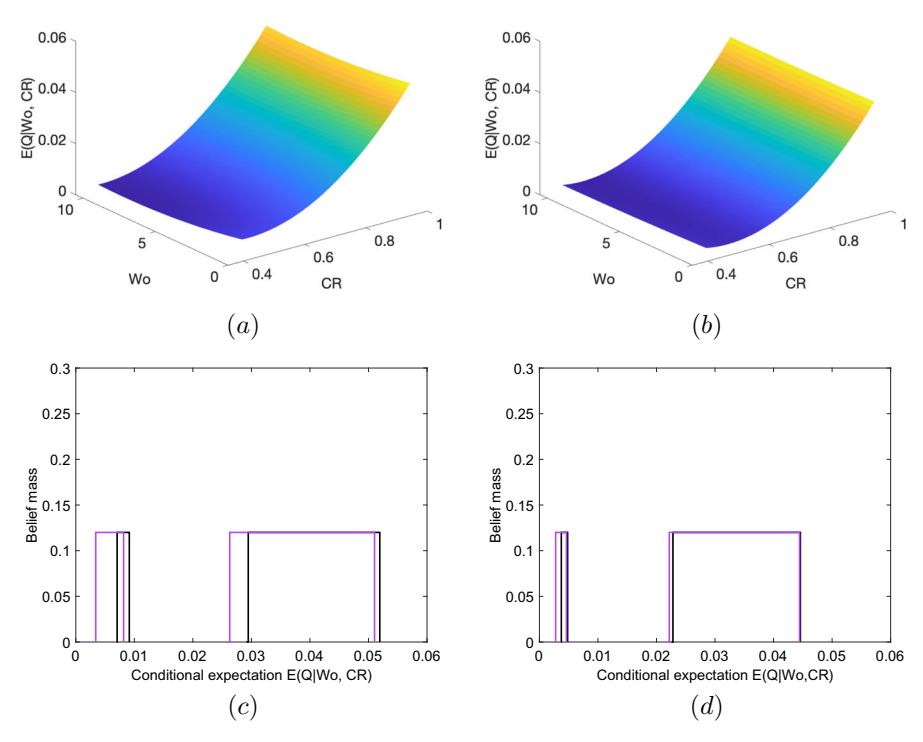


Fig. 11 Conditional expectation E(Q|Wo, CR): **a** surface—sine-wave model, **b** surface—pinch model, **c** focal elements with highest belief mass—sine-wave model, and **d** focal elements with highest belief mass—pinch model

#### 5.3 Flow characteristics comparison between peristalsis models

For the comparison purposes, we have provided the surfaces and m-functions (focal elements with the highest belief mass) for the expectation of flow volume rate from the two peristalsis models with sine-wave and Gaussian pinch wave, respectively (See Fig. 11). The left side figures are for sine-wave model while the right side figures are for pinch model. From the top surface plots, one can observe that flow volume rate from both models varies more along the CR direction compare to the Wo direction. Another observation is that when  $CR \in [0.4, 0.5)$ , the changing rate of  $E(Q|W_0, CR)$ for sine-wave model is relatively larger than the one for pinch model, which indicates the larger span in the corresponding output ranges. This observation is reflected in the two focal elements (corresponding to  $CR \in [0.4, 0.5)$ ) of the m-functions (bottom plots), i.e., the focal elements (towards to "0" side) for sine-wave model have larger size than the ones for pinch model. In addition, for a fixed  $CR \in [0.8, 0.95)$ , one can also observe from the surface plots that flow volume rate varies slightly more along Wo direction in sine-wave model compared to that in pinch model. This is reflected by the deviation of purple color focal elements from the blue color focal elements (toward to "0.06" side), i.e., the focal elements (in blue and purple color) overlaps less for sine-wave model compared to pinch model. Based on the observations (heuristic



13 Page 24 of 33 Y. He et al.

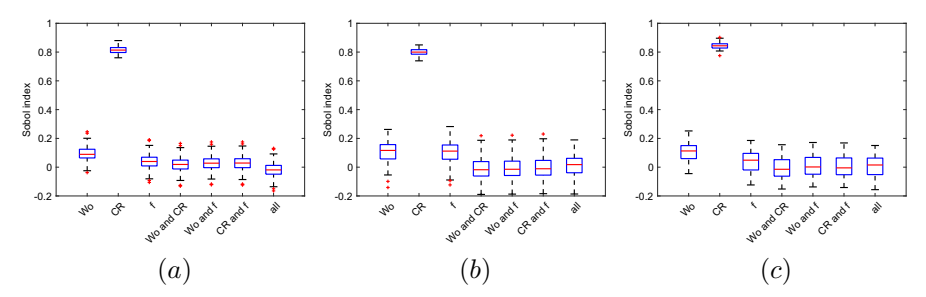


**Fig. 12** Boxplot of 100 trials Sobol' indices for pinch cost of transport with the assumptions of: **a** uniform distribution, **b** left quadratic distribution, and **c** right quadratic distribution over each focal elements

analysis), one may have some expectations regarding sensitivity: for both models, Q is very likely to be more sensitivity to CR compared to Wo; between these two models, it is possible for Wo to have a slightly more impact on Q from sine-wave model than the one from pinch model.

# 5.4 Sensitivity analysis

To further investigate the relation between OoIs and the input factors, and study the impact of uncertainty in input parameters on the model output, we implement the global sensitivity analysis with the method introduced in Sect. 4.3. Specifically, we calculate the Sobol' indices under three assumption of uniform, left quadratic and right quadratic distribution for uncertain variables in each focal element. For each of the three assumed distributions, MC method has been implemented with 1,000,000 sample size. We ran 100 experimental trials, and the boxplots of the obtained Sobol' indices are plotted in Fig. 12 for COT from pinch wave model as an example. Figure 12a illustrates the Sobol' indices under assumption of uniform distribution. Inside the figure, the center mark (red color) in each box is the median, the edges of the box are the 25th and 75th percentiles, the whiskers extend to the most extreme datapoints under consideration, and the excluded outliers are plotted individually. The results under assumptions of left quadratic and right quadratic distributions are provided in Fig. 12b, c, respectively. From the figures, one can conclude that the variation of CR has the most impact on the cost of transport for the pinch wave model for all the considered density distributions. In the remaining of this section, we will provide the bar graph representation of the median Sobol' indices from all three distributions together in one plot.

Using the same pinch model COT as an example, we provide the convergence of Sobol' indices calculated with all three representative distributions with respect to the sample size (see Fig. 13). The curves with different colors in all figures represent three uncertain inputs and their four interactions. One can observe that the ranking of "important" input factors (or their interactions) becomes reliable with a few thousands of samples, and the Sobol' indices (precise numbers) are converged before reaching our implementation sample size 1,000,000.

The Sobol' indices for volume flow rate from both sine-wave and pinch models are plotted in Fig. 14. In each plot, the indices with assumption of uniform distribution



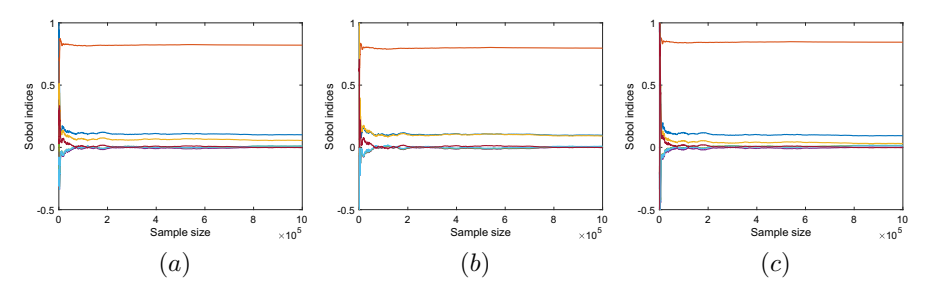


**Fig. 13** Convergence of Sobol's indices for pinch COT with respect to sample size: **a** uniform distribution, **b** left quadratic distribution, and **c** right quadratic distribution over each focal elements

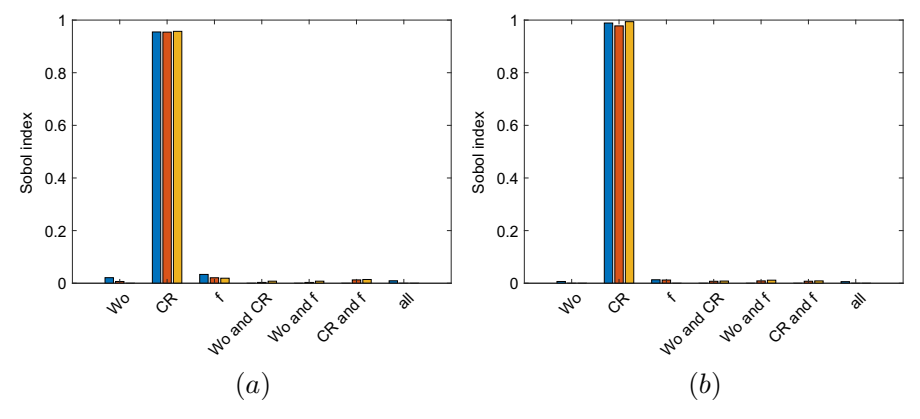


Fig. 14 Sobol' indices for volume flow rate: a with sine-wave model, and b with pinch model

(in each focal element) are visualized in blue color (left) bars, the ones with assumption of left quadratic distribution are shown in red color (middle) bars, while right quadratic distribution is corresponding to the orange bars (right). The conclusion that compression ratio CR has the most impact on the volume flow rate can be drawn regardless of the assumption of distributions inside focal elements and of the models. This is consistent with the previous study on experimental and analytical studies of peristalsis where the wave speed is decoupled from the compression frequency (Waldrop and Miller 2016). It also matches our expectation from the heuristic analysis in Sect. 5.3. The impact of other variables (or the combination of variables) on the flow is negligible compared to compression ratio.

The Sobol' indices for the energetic costs (work and COT) from both sine-wave and pinch models are plotted in Fig. 15. The top row of the figure shows that the work done on the tube during pumping is strongly influenced by Wo and f. For the sine-wave model of peristalsis, work is relatively more sensitive to f. While for pinch model, work is slightly more sensitive to Wo. For both models, work is also sensitive to the interaction of Wo and f. The afore-mentioned conclusions are consistent for the assumptions of all three distributions. The bottom row shows the sensitivity analysis of COT with respect to the three individual factors and their interactions. One can



13 Page 26 of 33 Y. He et al.

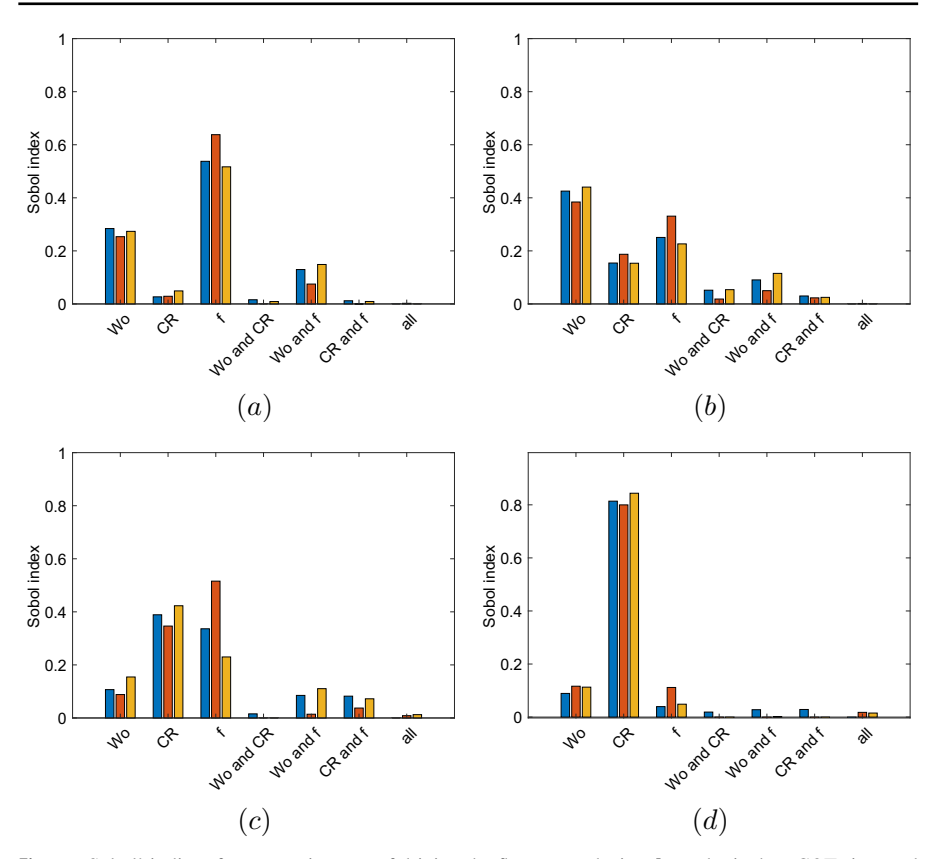


Fig. 15 Sobol' indices for energetic costs of driving the flow: a work sine, b work pinch, c COT sine, and d COT pinch

observe that COT is most sensitive to CR in pinch model while more sensitive to both CR and f in sine wave model.

This difference in sensitivity patterns in COT between the two pumping models is likely due to difference in mechanism. The sine-wave peristalsis assigns preferred motion to the majority of the active region of the tube, spreading the force required to compress the tube along a greater region. In comparison, the Gaussian-wave model assigns preferred motion to only the peak region, likely making this type of compression more expensive relative to compression ratio than the other method.

#### 5.5 Model reduction with SA

In our current work, we have first constructed gPC expansions as surrogates, and then implement uncertainty propagation and sensitivity analysis separately (can be in any order or simultaneously). However, when the dimension of uncertain input space is large, sensitivity analysis can be implemented first to identify "important" uncertain parameters. The remaining ones can then become deterministic with a fixed value since



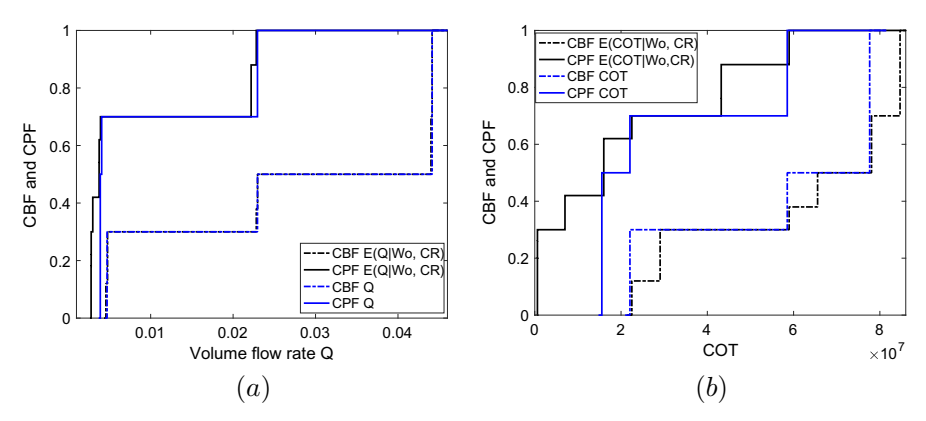


Fig. 16 CBF and CPF for pinch model: a volume flow rate Q, and b COT

their variations do not contribute as much to the uncertainty in outputs. Consequently, the dimension of uncertain input space an be reduced as well as the complexity of the problem. As mentioned in Sect. 4.1, the mixed UQ algorithm requires to solve a pair of optimization problems over each focal element (hypercube) of high-dimensional belief structure. Not only the dimension of each optimization space increases along with the number of uncertain input associated with belief functions, but also the number of focal elements over whole epistemic uncertain space (consequently, the number of optimization problems) increases exponentially along with it. Therefore, it is possible to reduce the computational cost exponentially with the help of sensitivity analysis.

For the purposes of illustration, we have taken pinch model as examples and analyzed the uncertainty in volume flow rate Q and cost of transport COT. From the sensitivity analysis results (Figs. 14b and 15d), the uncertainty in CR has the most impact on both Q and COT, where the latter one also has certain level of dependence on Wo and frequency. In this numerical experiment, we consider CR as the only uncertain variable, and fixed Wo= 1, f=1.25. The propagated uncertainties in Q and COT are represented with the CBFs/CPFs (Fig. 16 blue curves), compared to the ones with full dimension of original uncertain space (Fig. 16 black curves). The left figure is for volume flow rate Q while the fight figure is for cost of transport. As expected, the one for flow volume rate Q almost represents the full uncertainty, while the one for COT requires some compromise in accuracy.

#### 6 Discussion and conclusions

In this work, we introduce the theoretical basics from DS theory, present the numerical approach based on DS theory combined with MC sampling for mixed types of uncertainty propagation, and apply the approach to the computational model of peristalsis heart pumping system. To reduce the computational cost of MC method in stochastic uncertainty propagation process and the cost of the sampling method based optimizations in epistemic uncertainty propagation, gPC method is adopted to construct a cheaper surrogate to approximate the full simulations. With the approach, the mixed



13 Page 28 of 33 Y. He et al.

uncertainty in QoIs of computational model of peristalsis has been represented using belief structures (CBFs/CPFs) for the conditional expectation and standard deviation, which help to provide more information on QoIs such as the lower/upper bounds for the true possible probability of any propositions on QoIs. To further analyze the relation between the QoIs and uncertain input factors, we have implemented exploratory global sensitivity analysis in the framework of DS theory. The impact of the uncertainty in each individual input factors and their interactions on the QoIs are studied and compared between two peristalsis models.

The introduced mixed UQ method is comprehensive since it deals with both stochastic and epistemic uncertainties with different types. Thus, it is capable of uncertainty analysis for general biological models involving different types of uncertainties. In addition, the method considers the simulation of heart tube flow as a black box, the non-intrusive nature makes it ready to be applied to a more general simulation-based setting from various fields of applications. However, it can become computational expensive for complex problems with high-dimensional uncertain input space since the number of optimization problems increases exponentially along with the dimension as mentioned in Sect. 5.5. To reduce the computational cost, one may implement the sensitivity analysis for model reduction first, explore more efficient global optimization algorithms, and/or adopt efficient surrogate methods for high-dimensional problems. In addition, the exploratory global sensitivity analysis uses three representative probability density functions that are compatible with the belief structure and calculate the Sobol' indices using Monte Carlo method in the framework of probability theory. This extension (in the framework of Dempster-Shafer theory) is easy to understand and implement, which makes it convenient to be applied to systems involving epistemic uncertainty to identify "important" uncertain (both probabilistic and non-probabilistic) input factors.

In terms of the animal system, the current results suggest that the physical mechanism of driving flow is very important for understanding the underlying pattern of parameter sensitivity. While both pumping models produced similar patterns of sensitivity in terms of volume flow rate, these patterns were different for cost of transport. The physical mechanism of pumping for many tunicates and other tubular hearts is likely much closer to the Gaussian-wave peristalsis, having a sharp point of contraction that travels down an otherwise flexible heart tube. In this case, the cost of transport was much more sensitive to compression ratio than for the sine-wave model. The physical mechanism of pumping, therefore, is critically important to the overall conclusions of a parameter study and should be chosen carefully.

**Acknowledgements** This work was supported by National Science Foundation (DMS-2152040) and (DMS-2152110).

**Author Contributions** Y.H. conceived of the study, created the model, analyzed results, wrote the paper; N.A.B. analyzed results, wrote the paper; L.D.W. wrote the model, ran simulations, analyzed results, wrote the paper.

**Data availability** The raw data produced by the simulation code are provided at the following locations: visualization data and hierarchy data for pinch model (Waldrop et al. 2020g, h, c, d); visualization data and hierarchy data for sine-wave model (Waldrop et al. 2020i, j, e, f). The analyzed data can be found publicly at Waldrop et al. (2020b) the pinch model and Waldrop et al. (2020a) for the sine-wave model.



#### **Declarations**

**Conflict of interest** The authors declare no conflict of interest.

#### References

- Abdallah NB, Mouhous-Voyneau N, Denoeux T (2013) Using Dempster–Shafer theory to model uncertainty in climate change and environmental impact assessments. In: Proceedings of the 16th international conference on information fusion, Istanbul, Turkey, pp 2117–2124
- Anderson P, Patek SN (2015) Mechanical sensitivity reveals evolutionary dynamics of mechanical systems. Proc R Soc Lond B Biol Sci 282:20143088
- Arachchilage KH, Hussaini MY, Cogan NG, Cortez MH (2023) Exploring how ecological and epidemiological processes shape multi-host disease dynamics using global sensitivity analysis. J Math Biol 86(83):66
- Atkinson WD, Gammerman A (1987) An application of expert systems technology to biological identification. Taxon 36(4):705–714
- Bae HR, Grandhi RV, Canfield RA (2003) Uncertainty quantification of structural response using evidence theory. AIAA J 41(10):2062–2068
- Baird A, King T, Miller LA (2014) Numerical study of scaling effects in peristalsis and dynamic suction pumping. In: Layton AT, Olson SD (eds) Biological fluid dynamics: modeling, computations, and applications, pp 129–148. American Mathematical Society, Providence
- Baird A, Waldrop L, Miller L (2015) Neuromechanical pumping: boundary flexibility and traveling depolarization waves drive flow within valveless, tubular hearts. Jpn J Ind Appl Math 32(3):829–846. https://doi.org/10.1007/s13160-015-0195-3
- Battista NA, Lane AN, Miller LA (2017a) On the dynamic suction pumping of blood cells in tubular hearts. In: Layton AT, Miller LA (eds) Women in mathematical biology. Springer, Cham, pp 211–231
- Battista NA, Lane AN, Liu J, Miller LA (2017) Fluid dynamics in heart development: effects of hematocrit and trabeculation. Math Med Biol J IMA 35(4):493–516. https://doi.org/10.1093/imammb/dqx018
- Baudrit C, Dubois D, Guyonnet D (2006) Joint propagation and exploitation of probabilistic and possibilistic information in risk assessment. IEEE Trans Fuzzy Syst 14(5):593–608
- Bone Q, Inoue I, Tsutsui I (1997) Contraction and relaxation in the absence of a sarcoplasmic reticulum: muscle fibres in the small pelagic tunicate doliolum. J Muscle Res Cell Motil 18(3):375–380
- Cameron R, Martin W (1947) The orthogonal development of nonlinear functionals in series of Fourier–Hermite functionals. Ann Math 48(2):385–392
- Chen X, He Y, Xiu D (2015) An efficient method for uncertainty propagation using fuzzy sets. SIAM J Sci Comput 37(6):2488–2507
- Childs H, Brugger E, Whitlock B, Meredith J, Ahern S, Pugmire D, Biagas K, Miller M, Harrison C, Weber GH, Krishnan H, Fogal T, Sanderson A, Garth C, Bethel EW, Camp D, Rübel O, Durant M, Favre JM, Navrátil P (2012) Visit: an end-user tool for visualizing and analyzing very large data. In: Bethel EW, Childs H, Hansen C (eds) High performance visualization-enabling extreme-scale scientific insight. Chapman and Hall/CRC, Boca Raton, pp 357–372
- Dempster AP (1967) Upper and lower probabilities induced by a multi-valued mapping. Ann Math Stat 38:325–339
- Denaeux T (2009) Extending stochastic ordering to belief functions on the real line. Inf Sci 179:1362–1376
  Destercke S, Dubois D, Chojnachi E (2008) Unifying practical uncertainty representations: I. Generalized p-boxes. Int J Approx Reason 49:649–663
- Dubois D (2006) Possibility theory and statistical reasoning. Comput Stat Data Anal 51(1):47-69
- Dubois D, Prade H (1988) Possibility theory: an approach to computerized processing of uncertainty. Plenum Press, New York
- Dubois D, Prade H (1991) Random sets and fuzzy interval analysis. Fuzzy Sets Syst 42:87-101
- Eldred MS, Swiler LP, Tang G (2011) Mixed aleatory-epistemic uncertainty quantification with stochastic expansions and optimization-based interval estimation. Reliab Eng Syst Saf 96:1092–1113
- Forouhar AS, Liebling M, Hickerson A, Nasiraei-Moghaddam A, Tsai H-J, Hove JR, Fraser SE, Dickinson ME, Gharib M (2006) The embryonic vertebrate heart tube is a dynamic suction pump. Science 312(5774):751–753. https://doi.org/10.1126/science.1123775



13 Page 30 of 33 Y. He et al.

Fung YC, Yih CS (1968) Peristaltic transport. ASME J Appl Mech 35(4):669–675. https://doi.org/10.1115/

- Gashev AA (2002) Physiologic aspects of lymphatic contractile function. Ann N Y Acad Sci 979(1):178–187. https://doi.org/10.1111/j.1749-6632.2002.tb04878.x
- Ghanem RG, Spanos PD (1991) Stochastic finite elements: a spectral approach. Springer, New York
- Glenn JD, King JG, H JF (2010) Structural mechanics of the mosquito heart and its function in bidirectional hemolymph transport. J Exp Biol 213(4):541–550. https://doi.org/10.1242/jeb.035014
- Goodman IR, Nguyen HT (1985) Uncertainty models for knowledge-based systems: a unified approach to the measurement of uncertainty. Elsevier, New York
- Griffith B (2014) An adaptive and distributed-memory parallel implementation of the immersed boundary (IB) method (IBAMR). https://github.com/IBAMR/IBAMR
- Griffiths DJ, Constantinou CE, Mortensen J, Djurhuus JC (1987) Dynamics of the upper urinary tract: II.

  The effect of variations of peristaltic frequency and bladder pressure on pyeloureteral pressure/flow relations. Phys Med Biol 32(7):823. https://doi.org/10.1088/0031-9155/32/7/003
- He Y, Hussaini MY (2023) Mixed aleatory and epistemic uncertainty propagation using Dempster–Shafer theory. J Comput Appl Math 429:115234. https://doi.org/10.1016/j.cam.2023.115234
- He Y, Mirzargar M, Kirby RM (2015) Mixed aleatory and epistemic uncertainty quantification using fuzzy set theory. Int J Approx Reason 66:1–15
- He Y, Razi M, Forestiere C, Dal Negro L, Kirby RM (2018) Uncertainty quantification guided robust design for nanoparticles' morphology. Comput Methods Appl Mech Eng 336:578–593. https://doi.org/10.1016/j.cma.2018.03.027
- He Y, Chilleri J, O'Leary SK, Shur MS, Kirby RM (2020) Sensitivity analysis for an electron transport system: application to the case of wurtzite gallium nitride. J Comput Electron 19:103–110
- Helton JC, Johnson JD, Oberkampf WL, Sallaberry CJ (2006) Sensitivity analysis in conjunction with evidence theory representations of epistemic uncertainty. Reliab Eng Syst Saf 91(10):1414–1434
- Heron A (1973) A specialized predator–prey relationship between the copepod *Sapphirina angusta* and the pelagic tunicate thalia democratica. J Mar Biol Assoc UK 53(2):429–435
- Hu N, Clark E (1989) Hemodynamics of the stage 12 to stage 29 chick embryo. Circ Res 65(6):1665–1670 Hu Z, Du D, Du Y (2018) Generalized polynomial chaos-based uncertainty quantification and propagation in multi-scale modeling of cardiac electrophysiology. Comput Biol Med 102:57–74
- Jaffrin MY, Shapiro AH (1971) Peristaltic pumping. Annu Rev Fluid Mech 3(1):13–37. https://doi.org/10. 1146/annurev.fl.03.010171.000305
- Jakeman J, Eldred M, Xiu D (2010) Numerical approach for quantification of epistemic uncertainty. J Comput Phys 229:4648–4663
- Jarrett AM, Liu Y, Cogan NG, Hussaini MY (2015) Global sensitivity analysis used to interpret biological experimental results. J Math Biol 71:151–170
- Jones EAV, Baron MH, Fraser SE, Dickinson ME (2004) Measuring hemodynamic changes during mammalian development. Am J Physiol Heart Circ Physiol 287(4):1561–1569. https://doi.org/10.1152/ajpheart.00081.2004
- Jung E, Peskin CS (2001) Two-dimensional simulations of valveless pumping using the immersed boundary method. SIAM J Sci Comput 23(1):19–45. https://doi.org/10.1137/S1064827500366094
- Kalk M (1970) The organization of a tunicate heart. Tissue Cell 2(1):99-118
- Kiparissides A, Rodriguez-Fernandez M, Kucherenko S, Mantalaris A, Pistikopoulos E (2008) Application of global sensitivity analysis to biological models. In: Braunschweig B, Joulia X (eds) 18th European symposium on computer aided process engineering, vol 25. Computer Aided Chemical Engineering, pp 689–694
- Konrad MW (2016) Blood circulation in the ascidian tunicate corella inflata (corellidae). PeerJ 4:2771
- Kozlovsky P, Bryson-Richardson RJ, Jaffa AJ, Rosenfeld M, Elad D (2016) The driving mechanism for unidirectional blood flow in the tubular embryonic heart. Ann Biomed Eng 44(10):3069–3083. https:// doi.org/10.1007/s10439-016-1620-8
- Lee W, Lim S, Jung E (2012) Dynamical motion driven by periodic forcing on an open elastic tube in fluid. Commun Comput Phys 12:494–513
- Lockwood B, Anitescu M, Mavripilis F (2012) Mixed aleatory/epistemic uncertainty quantification for hypersonic flows via gradient-based optimization and surrogate models. In: Proceedings of the 50th AIAA aerospace sciences meeting, AIAA2012-1254, Nashville, TN



- Männer J, Wessel A, Yelbuz TM (2010) How does the tubular embryonic heart work? Looking for the physical mechanism generating unidirectional blood flow in the valveless embryonic heart tube. Dev Dyn 239(4):1035–1046. https://doi.org/10.1002/dvdy.22265
- Marino S, Hogue IB, Ray CJ, Kirschner DE (2008) A methodology for performing global uncertainty and sensitivity analysis in systems biology. J Theor Biol 254(1):178–196
- Mathelin L, Hussaini MY (2003) A stochastic collocation algorithm for uncertainty analysis. Technical Report NASA/CR-2003-212153, NASA Langley Research Center
- Midgett M, Goenezen S, Rugonyi S (2014) Blood flow dynamics reflect degree of outflow tract banding in Hamburger–Hamilton stage 18 chicken embryos. J R Soc Interface 11(100):20140643
- Mitra ED, Hlavacek WS (2019) Parameter estimation and uncertainty quantification for systems biology models. Curr Opin Syst Biol 18:9–18
- Muñoz MM (2019) The evolutionary dynamics of mechanically complex systems. Integr Comp Biol 59:705–715
- Nguyen HT (1978) On random sets and belief functions. J Math Anal Appl 65:531-542
- Oberkampf WL, Helton JC, Sentz K (2001) Mathematical representation of uncertainty. In: Proceedings of the AIAA non-deterministic approaches forum AIAA 2001-1645, Seattle, WA
- Polly PD, Stayton CT, Dumont ER, Pierce SE, Rayfield EJ, Angielczyk KD (2016) Combining geometric morphometrics and finite element analysis with evolutionary modeling: towards a synthesis. J Vertebr Paleontol 36:1111225
- Pozrikidis C (1987) A study of peristaltic flow. J Fluid Mech 180:515–527. https://doi.org/10.1017/ S0022112087001939
- Quarteroni A, Manzoni A, Vergara C (2017) The cardiovascular system: mathematical modeling, numerical algorithms and clinical applications. Acta Numer 26:365–590
- R Core Team (2021) R: a language and environment for statistical computing. R Foundation for Statistical Computing, Vienna, Austria
- Randall EB, Randolph NZ, Alexanderian A, Olufsen MS (2021) Global sensitivity analysis informed model reduction and selection applied to a valsalva maneuver model. J Theor Biol 526:110759
- Regan HM, Colyvan M, Burgman MA (2002) A taxonomy and treatment of uncertainty for ecology and conservation biology. Ecol Appl 12(2):618–628. https://doi.org/10.1890/1051-0761(2002)012[0618: ATATOU]2.0.CO;2
- Roy CJ, Oberkampf WL (2011) A comprehensive framework for verification, validation, and uncertainty quantification in scientific computing. Comput Methods Appl Mech Eng 200:2131–2144
- Schobi R, Sudret B, Wiart J (2015) Polynomial-chaos-based kriging. Int J Uncertain Quantif 5:171–193 Shafer G (1976) A mathematical theory of evidence. Princeton University Press, NJ
- Shah H, Hosder S, Winter T (2015) A mixed uncertainty quantification approach using evidence theory and stochastic expansions. Int J Uncertain Quantif 5(1):21–48
- Shapiro AH, Jaffrin MY, Weinberg SL (1969) Peristaltic pumping with long wavelengths at low Reynolds number. J Fluid Mech 37(4):799–825. https://doi.org/10.1017/S0022112069000899
- Sobol' IM (1993) Sensitivity estimates for nonlinear mathematical models. Math Model Comput Exp 4:407–414
- Sobol' IM (2001) Global sensitivity indices for nonlinear mathematical models and their Monte Carlo estimates. Math Comput Simul 55(1):271–280. https://doi.org/10.1016/S0378-4754(00)00270-6. The second IMACS seminar on Monte Carlo methods
- Sobol' IM, Kucherenko S (2005) Global sensitivity indices for nonlinear mathematical models. Rev Wilmott Mag 01:56-61
- Sudret B (2008) Global sensitivity analysis using polynomial chaos expansions. Reliab Eng Syst Saf 93(7):964–979. https://doi.org/10.1016/j.ress.2007.04.002. Bayesian networks in dependability
- Swiler LP, Gulian M, Frankel AL, Safta C, Jakeman JD (2020) A survey of constrained gaussian process regression: approaches and implementation challenges. J Mach Learn Model Comput 1(2):119–156
- Taber LA (2001) Biomechanics of cardiovascular development. Annu Rev Biomed Eng 3(1):1–25. https://doi.org/10.1146/annurev.bioeng.3.1.1
- Taber LA, Zhang J, Perucchio R (2006) Computational model for the transition from peristaltic to pulsatile flow in the embryonic heart tube. J Biomech Eng 129(3):441–449. https://doi.org/10.1115/1.2721076
- Talavera A, Aguasca R, Galván B, no AC (2013) Application of Demster–Shafer theory for the quantification and propagation of the uncertainty caused by the use of ais data. Reliab Eng Syst Saf 111:95–105



13 Page 32 of 33 Y. He et al.

Tang G, Swiler LP, Eldred MS, Iaccarino G (2010) Using stochastic expansion methods in evidence theory for mixed aleatory-epistemic uncertainty quantification. In: Proceeding of the 12th AIAA non-deterministic approaches conference, Orlando, FL

- Tang J, Wu Z, Yang C (2015) Epistemic uncertainty quantification in flutter analysis using evidence theory. Chin J Aeronaut 28:897–936
- Tonon F, Bernardini A, Mammino A (1991) Reliability analysis of rock mass response by means of random set theory. Reliab Eng Syst Saf 42:263–282
- Wainwright PC (2007) Functional versus morphological diversity in macroevolution. Annu Rev Ecol Evol Syst 38(1):381–401
- Wainwright P, Alfaro M, Bolnick D, Hulsey C (2005) Many-to-one mapping to form to function: a general principle in organismal design? Integr Comp Biol 01:256–262
- Waldrop LD, Miller LA (2015) The role of the pericardium in the valveless, tubular heart of the tunicate Ciona savignyi. J Exp Biol 218(17):2753–2763. https://doi.org/10.1242/jeb.116863
- Waldrop L, Miller L (2016) Large-amplitude, short-wave peristalsis and its implications for transport. Biomech Model Mechanobiol 15(3):629–642. https://doi.org/10.1007/s10237-015-0713-x
- Waldrop LD, He Y, Khatri S (2018) What can computational modeling tell us about the diversity of odorcapture structures in the Pancrustacea? J Chem Ecol 44(12):1084–1100
- Waldrop L, Miller L, Battista N, He Y (2020a) Analyzed results of pinch model. https://doi.org/10.6084/m9.figshare.11819388.v1
- Waldrop L, Miller L, Battista N, He Y (2020b) Analyzed results of sine-wave model. https://doi.org/10. 6084/m9.figshare.11819439.v1
- Waldrop L, Miller L, Battista N, He Y (2020c) Lagrangian data (pinch model) simulations 1–500. https://doi.org/10.6084/m9.figshare.11819328.v2
- Waldrop L, Miller L, Battista N, He Y (2020d) Lagrangian data (pinch model) simulations 501–681. https://doi.org/10.6084/m9.figshare.11839227.v1
- Waldrop L, Miller L, Battista N, He Y (2020e) Lagrangian data (sine-wave model) simulations 1–500. https://doi.org/10.6084/m9.figshare.11819331
- Waldrop L, Miller L, Battista N, He Y (2020f) Lagrangian data (sine-wave model) simulations 501–681. https://doi.org/10.6084/m9.figshare.11839236.v1
- $Waldrop\ L, Miller\ L,\ Battista\ N,\ He\ Y\ (2020g)\ Viz\ dump\ data\ simulations\ (pinch\ model)\ simulations\ 1-500.$  https://doi.org/10.6084/m9.figshare.11782320.v10
- Waldrop L, Miller L, Battista N, He Y (2020h) Viz dump data simulations (pinch model) simulations 501–681. https://doi.org/10.6084/m9.figshare.11833047
- Waldrop L, Miller L, Battista N, He Y (2020i) Viz dump data simulations (sine-wave model) simulations 1–500. https://doi.org/10.6084/m9.figshare.11819313
- Waldrop L, Miller L, Battista N, He Y (2020j) Viz dump data simulations (sine-wave model) simulations 501–681. https://doi.org/10.6084/m9.figshare.11839191
- Waldrop LD, He Y, Battista NA, Neary PT, Miller LA (2020k) Uncertainty quantification reveals the physical constraints on pumping by peristaltic hearts. J R Soc Interface 17(170):20200232. https://doi.org/10.1098/rsif.2020.0232
- Walley P, Cooman GD (2001) A behavioural model for linguistic uncertainty. Inf Sci 134:1-37
- Wang C, Qiu Z, He Y (2015) Fuzzy interval perturbation method for the uncertain heat conduction problem with interval and fuzzy parameters. Int J Numer Methods Eng 104:330–346
- Wang C, Qiu Z, Xu M, Li Y (2017) Novel reliability-based optimization method for thermal structure with hybrid random, interval and fuzzy parameters. Appl Math Model 47:573–586. https://doi.org/ 10.1016/j.apm.2017.03.053
- Wiener N (1938) The homogeneous chaos. Am J Math 60:897-936
- Xavier-Neto J, Davidson B, Simoes-Costa MS, Castro RA, Castillo HA, Sampaio AC, Azambuja AP (2010) Chapter 1.1—evolutionary origins of hearts. In: Rosenthal N, Harvey RP (eds) Heart development and regeneration. Academic Press, Boston, pp 3–45. https://doi.org/10.1016/B978-0-12-381332-9. 00001-3
- Xiu D (2010) Numerical methods for stochastic computations: a spectral method approach. Princeton University Press, New Jersey
- Xiu D, Karniadakis GE (2002) The Wiener–Askey polynomial chaos for stochastic differential equations. SIAM J Sci Comput 24:619–644
- Xiu D, Karniadakis GE (2003) Modeling uncertainty in flow simulations via generalized polynomial chaos. J Comput Phys 187(1):137–167. https://doi.org/10.1016/S0021-9991(03)00092-5



Yager RR (2004) Cumulative distribution functions from Dempster–Shafer belief structures. IEEE Tran Syst Man Cybernet 34(5):2080–2087

Zadeh LA (1965) Fuzzy sets. Inf Control 8:338-353

**Publisher's Note** Springer Nature remains neutral with regard to jurisdictional claims in published maps and institutional affiliations.

Springer Nature or its licensor (e.g. a society or other partner) holds exclusive rights to this article under a publishing agreement with the author(s) or other rightsholder(s); author self-archiving of the accepted manuscript version of this article is solely governed by the terms of such publishing agreement and applicable law.

